Neutrino and antineutrino charge-exchange reactions on ^{12}C

A. R. Samana,[1,2,*] F. Krmpotić,[3] N. Paar,[4] and C. A. Bertulani[1]

[1]*Department of Physics, Texas A&M University Commerce, P.O. Box 3011 Commerce, Texas 75429, USA*

[2]*Departamento de Ciências Exactas e Tecnológicas, Universidade Estadual de Santa Cruz, CEP 45662-000, Ilheús, Bahia-BA, Brazil*

[3]*Instituto de Física La Plata, CONICET, Facultad de Ciencias Astronómicas y Geofísicas, Universidad Nacional de La Plata, 1900 La Plata, Argentina*

[4]*Physics Department, Faculty of Science, University of Zagreb, Bijenicka 32, HR-10002 Zagreb, Croatia*

(Received 12 May 2010; revised manuscript received 26 November 2010; published 9 February 2011)

We extend the formalism of weak interaction processes, obtaining new expressions for the transition rates, which greatly facilitate numerical calculations, for both neutrino-nucleus reactions and muon capture. Explicit violation of the conserved vector current hypothesis by the Coulomb field, as well as development of a sum-rule approach for inclusive cross sections, has been worked out. We have done a thorough study of exclusive (ground-state) properties of ^{12}B and ^{12}N within the projected quasiparticle random phase approximation (PQRPA). Good agreement with experimental data achieved in this way put into evidence the limitations of the standard RPA and QRPA models, which come from the inability of the RPA to open the $p_{3/2}$ shell and from the nonconservation of the number of particles in the QRPA. The inclusive neutrino/antineutrino ($\nu/\tilde{\nu}$) reactions ^{12}C$(\nu, e^-)^{12}$N and ^{12}C$(\tilde{\nu}, e^+)^{12}$B are calculated within both the PQRPA and the relativistic QRPA. It is found that (i) the magnitudes of the resulting cross sections are close to the sum-rule limit at low energy, but significantly smaller than this limit at high energies, for both ν and $\tilde{\nu}$; (ii) they increase steadily when the size of the configuration space is augmented, particularly for $\nu/\tilde{\nu}$ energies >200 MeV; and (iii) they converge for sufficiently large configuration space and final-state spin. The quasi-elastic ^{12}C$(\nu, \mu^-)^{12}$N cross section recently measured in the MiniBooNE experiment is briefly discussed. We study the decomposition of the inclusive cross section based on the degree of forbiddenness of different multipoles. A few words are dedicated to the $\nu/\tilde{\nu}$-^{12}C charge-exchange reactions related to astrophysical applications.

DOI: 10.1103/PhysRevC.83.024303 PACS number(s): 23.40.−s, 25.30.Pt, 26.50.+x

I. INTRODUCTION

The massiveness of neutrinos and related oscillations are strongly sustained by many experimental works involving atmospheric, solar, reactor, and accelerator neutrinos [1–7]. The subsequent experimental goal is to determine precisely the various parameters of the Pontecorvo-Maki-Nakagawa-Sakata (PMNS) neutrino mass matrix, absolute masses of different flavors of neutrinos, CP violation in the neutrino sector, etc. To address these problems several analyses of neutrino oscillation data are presently ongoing. At the same time, several experiments are currently collecting data, and others are planned. Accelerator experiments and experiments with neutrinos from ν factories, β beams, etc., are also planned and designed, as well as some experiments with natural ν sources like solar neutrinos, atmospheric neutrinos, and antineutrinos from nuclear reactors.

Neutrino-nucleus scattering in ^{12}C is important because this nucleus is a component of many liquid scintillator detectors. Experiments such as LSND [1,2], KARMEN [8,9], and LAMPF [10,11] have used ^{12}C to search for neutrino oscillations and to measure neutrino-nucleus cross sections. Present atmospheric and accelerator-based neutrino oscillation experiments also involve ^{12}C and operate at neutrino energies $E_\nu \sim 1$ GeV to access the relevant regions of the oscillation parameter space. This is the case of the SciBar detector [12], where the C_8H_8 molecule is involved, and the MiniBooNE detector [13], which uses the light mineral oil containing the CH_2 molecule. The ^{12}C target will be used in several planned experiments, such as the spallation neutron source (SNS) at Oak Ridge National Laboratory [14] and the LVD (Large Volume Detector) experiment [15], developed by the INFN in Gran Sasso.

For the planned experimental searches of supernova neutrino signals, which involve ^{12}C as scintillator liquid detector, the precise knowledge of neutrino cross sections of ^{12}N and ^{12}B ground states, that is, of $\sigma_{e^-}(E_\nu, 1^+_1)$ and $\sigma_{e^+}(E_{\tilde{\nu}}, 1^+_1)$, is very important. In fact, in the LVD experiment [15] the number of events detected during the supernova explosion are estimated by convoluting the neutrino supernova flux with (i) the interaction cross sections, (ii) the efficiency of the detector, and (iii) the number of target nuclei. So far $\sigma_{e^-}(E_\nu, 1^+_1)$ and $\sigma_{e^+}(E_{\tilde{\nu}}, 1^+_1)$, as obtained from the elementary particle treatment (EPT), have been used for the carbon content of the LVD [16]. Moreover, as an update of the LVD experiment related to supernova neutrino detection (where ^{12}C is also employed), a design study concerning large scintillator detectors, called LAGUNA, where a 50-kt scintillator LENA is being considered, is ongoing [17].

On the other hand, as the ^{12}C nucleus forms one of the onion-like shells of a large star before collapse, it is also important for astrophysics studies. Concomitantly, several authors [15,18–23] have recently stressed the importance of measuring supernova neutrino oscillations. They claim that a

*arturo.samana@gmail.com

supernova explosion represents a unique scenario for further study of the PMNS matrix. The corresponding neutrinos, which carry all flavors, have been observed on only one occasion (SN1987A), have an energy $E_\nu \lesssim 100$ MeV [24], and are also studied through the interactions with carbon nuclei in the liquid scintillator.

Thus, the main interest in the neutrino/antineutrino-^{12}C charge-exchange cross sections lies in the neutrino oscillations, and precise knowledge of cross sections in neutrino energies going from a few MeVs up to a few giga–electron volts is required. Until quite recently the only available experimental information on reactions was that for flux-averaged cross sections: (i) $E_{\nu_e} < 60$ MeV for $^{12}\mathrm{C}(\nu_e, e^-)^{12}\mathrm{N}$ in the DAR region [25–27] and (ii) 127 MeV $\leqslant E_{\nu_\mu} \leqslant 300$ MeV for $^{12}\mathrm{C}(\nu_\mu, \mu^-)^{12}\mathrm{N}$ in the DIF region [28–30]. In the last few years, however, several experimental programs at MiniBooNE [31], K2K [32], and SciBooNE [33] have yielded results on the $(\nu_\mu, ^{12}\mathrm{C})$ cross section for 0.4 GeV $\leqslant E_{\nu_\mu} \leqslant 1.7$ GeV. It is well known that for E_ν higher than a few hundred MeV's, besides the quasielastic (QE) channel, many inelastic channels are open and pion production becomes important. In fact, there have been quite active experimental efforts to investigate neutrino-induced coherent single-pion production in the Δ-excitation region of ^{12}C. Starting approximately at the threshold coming from the pion and charged lepton masses (m_π and m_ℓ), the $\pi + \ell$ production cross section steadily increases, with the neutrino energy becoming higher than the QE one for $E_\nu \lesssim 1.5$ GeV [31–33].

On the theoretical side there have been great efforts to understand the nuclear structure within the triad $\{^{12}\mathrm{B}, ^{12}\mathrm{C}, ^{12}\mathrm{N}\}$. In the seminal work by O'Connell, Donelly, and Walecka [34], a unified analysis of electromagnetic and semileptonic weak interactions was presented. To describe the nuclear dynamics they have used the particle-hole Tamm-Dancof approximation (TDA) within a very small single-particle (s.p.) space[1] ($S_2 \equiv \{1s_{1/2}, 1p_{3/2}, 1p_{1/2}, 1d_{5/2}, 2s_{1/2}\}$) [35]. To achieve agreement with experiments for $\beta^\pm$ decays and μ capture, they were forced to use an overall reduction factor ξ^2 of the order of 4 (2) for even (odd) parity states. They have also pointed out that this factor would become totally unnecessary with the use of a better nuclear model able to open the $1p_{3/2}$ shell.

Rather thorough comparisons of $2s1d$ and $2p1f$ shell-model (SM) predictions with measured allowed β-decay rates have yielded a simple, phenomenological effective axial coupling $g_A = 1$ that should be used rather than the bare value [36–39]. This observation is the basis for many nuclear model estimates of the Gamow-Teller (GT) response that governs allowed neutrino cross sections. In Ref. [34], $g_A = 1.23$ was used, based on a study of neutron β decay, and as the analyzed processes were dominantly of the axial-vector type, the use of $g_A = 1$ would have diminished the reduction factors ξ^2 in an appreciable way.

In the random phase approximation (RPA), besides the TDA forward-going amplitudes, backward-going amplitudes are present as well. However, these additional RPA amplitudes did not help to open the $1p_{3/2}$ shell in the continuum RPA (CRPA) calculations of Kolbe, Langanke, and Krewald [40]. Thus, as in the case of the TDA used in Ref. [34], to get agreement with data for the ground-state triplet $T = 1$ [$\beta^\pm$ decays, μ capture, and the exclusive $^{12}\mathrm{C}(\nu_e, e^-)^{12}\mathrm{N}$ reaction], their calculations were rescaled by a factor of $\cong$4.

The main aim of the CRPA is to describe appropriately not only the bound states but also the virtual (quasibound), resonant, and continuum states, which are treated as bound states in the RPA. However, this superiority has not been evidenced so far in numerical calculations. For instance, in the case of μ-capture rates in ^{16}N, the two methods agree with each other quite well for the 0^- and 1^- states, while the RPA result is preferred for the 2^- state [41].

To open the $1p_{3/2}$ shell, one has to introduce pairing correlations. This is done within the SM [42–44], which reproduces quite well both (i) the experimental flux-averaged exclusive cross section (ECS) and inclusive cross section (ICS) for the $^{12}\mathrm{C}(\nu_e, e^-)^{12}\mathrm{N}$ DAR [25–27] and $^{12}\mathrm{C}(\nu_\mu, \mu^-)^{12}\mathrm{N}$ DIF [28] reactions and (ii) the $\mu^- + ^{12}\mathrm{C} \rightarrow \nu_\mu + ^{12}\mathrm{B}$ muon-capture modes [45–47].

The quasiparticle RPA (QRPA) also opens the $1p_{3/2}$ shell by means of the pairing interaction. However, it fails as well in accounting for the exclusive processes triplet $T = 1$ in ^{12}C, because a new problem emerges, as first observed by Volpe *et al.* [43]. They noted that within the QRPA the lowest state in ^{12}N irremediably turned out not to be the most collective one. Later it was shown [48–50] that (1) the origin of this difficulty arises from the degeneracy among the four lowest proton-neutron two-quasiparticle ($2qp$) states $|1p_{1/2}1p_{3/2}\rangle$, $|1p_{3/2}1p_{3/2}\rangle$, $|1p_{1/2}1p_{1/2}\rangle$, and $|1p_{3/2}1p_{1/2}\rangle$, which, in turn, comes from the fact that for $N = Z = 6$ the quasiparticle energies $E_{1p_{1/2}}$ and $E_{1p_{3/2}}$ are very close to each other; and (2) it is imperative to use the projected QRPA (PQRPA) for a physically sound description of the weak processes among the ground states of the triad $\{^{12}\mathrm{B}, ^{12}\mathrm{C}, ^{12}\mathrm{N}\}$ [48–50] (see Figs. 2 and 3 in Ref. [49]).

In summary, neither the CRPA nor the QRPA is the appropriate nuclear model to describe the "fine structure" of exclusive charge-exchange processes around ^{12}C, and they can only be used for global inclusive descriptions. Of course, the same is valid for the relativistic RPA (RQRPA), which has recently been applied with success in calculations of inclusive charged-current neutrino-nucleus reactions in ^{12}C, ^{16}O, ^{56}Fe, and ^{208}Pb [51] and total muon-capture rates in a large set of nuclei from ^{12}C to ^{244}Pu [52]. The continuum QRPA (CQRPA) would have to be superior to the QRPA for the same reasons that the CRPA would have to be better than the RPA. Nevertheless, this superiority has not been evidenced by numerical calculations [53,54]. Finally, it is clear that the nuclear structure descriptions inspired by the relativistic Fermi gas model (RFGM) [54–57], which do not involve multipole expansions, should only be used for inclusive quantities.

When the effects owing to resonant and continuum states are considered, as done within the CRPA and CQRPA, the spreading in strength of the hole states in the inner shells should also be taken into account for the sake of consistency. In fact, an s.p. state j that is deeply bound in the parent nucleus, after a weak interacting process, can become a highly excited

[1]Henceforth, a single-particle (s.p.) space that includes all orbitals within the N harmonic oscillator (HO) shells is labeled space S_N.

hole-state j^{-1} in the continuum of the residual nucleus. There it is suddenly mixed with more complicated configurations ($2h1p$, $3h2p$, . . ., excitations, collective states, and so on) spreading its strength over a relatively wide energy interval [58].[2] This happens, for instance, with the $1s_{1/2}$ orbital in ^{12}C, which is separated from the $1p_{3/2}$ state by approximately 23 MeV, which is enough to break the 12-particle system, where the energy of the last excited-state amounts to 11.5 MeV in ^{12}N and 16.5 MeV in ^{12}B channels. Although the detailed structure and fragmentation of hole states are still not well known, the exclusive knockout reactions provide a wealth of information on the structure of single-nucleon states of nuclei. Excitation energies and widths of proton-hole states were systematically measured with quasifree $(p, 2p)$ and $(e, e'p)$ reactions, which revealed the existence of inner orbital shells in nuclei [59–67].

In the TDA calculation in Ref. [34] the S_2 space has been used, which extends only from 13.77 up to 30.05 MeV, embracing, respectively, one, three, two, one, and one negative-parity states $J^\pi = 0^-, 1^-, 2^-, 3^-$, and 4^-, and one, two, two, and one positive-parity states $J^\pi = 0^+, 1^+, 2^+$, and 3^+. For such small configuration spaces, the neutrino cross sections $\sigma_e(E_\nu)$ and $\sigma_\mu(E_\nu)$ have been evaluated up to a neutrino energy E_ν of 0.6 GeV and extrapolated up to 20 GeV. In recent years, however, large configuration spaces have been used in the evaluation of QE cross sections for $E_\nu \sim 1$ GeV. For instance, Amaro *et al.* [68] have employed the s.p. SM (TDA without the residual interaction) in a semirelativistic description of QE neutrino reactions (ν_μ, μ^-) on ^{12}C going up to $E_\nu = 1.5$ GeV, and including multipoles $J^\pi \leqslant 47^\pm$. Good agreement with the RFGM was obtained for several choices of kinematics of interest for the ongoing neutrino oscillation experiments. Kolbe *et al.* [69] have also achieved an excellent agreement between RFGM and CRPA calculations of the total cross section and the angular distribution of the outgoing electrons in $^{16}\mathrm{O}(\nu_e, e)X$ for $E_\nu \leqslant 0.5$ GeV. They considered states up to $J^\pi = 9^\pm$ only, and did not specify the configuration space used. Moreover, Valverde *et al.* [54,57] have analyzed the theoretical uncertainties of the RFGM developed in Ref. [56] for (ν_e, e^-), and (ν_μ, μ^-) cross sections in ^{12}C, ^{16}O, and ^{40}Ca for $E_\nu \leqslant 0.5$ GeV. The work of Kim *et al.* [70] should also be mentioned, which studied the effects of strangeness on (ν_μ, μ^-) and $(\tilde{\nu}_\mu, \mu^+)$ cross sections in ^{12}C for incident energies between 0.5 MeV and 1.0 GeV, within the framework of a relativistic s.p. model. Quite recently, Butkevich [71] has also studied the scattering of muon neutrinos on carbon targets for neutrino energies up to 2.8 GeV within a relativistic SM approach without specifying the model space.

For relatively high neutrino energies ($E_{\nu e} \gtrsim \mathrm{m}_\pi$ and $E_{\nu_\mu} \gtrsim \mathrm{m}_\pi + \mathrm{m}_\mu$), the pion production cross section should be added to the aforementioned QE cross sections, as done, for instance, in Refs. [72] and [73]. One should also note that $\sigma_e(E_{\nu_e})$ and $\sigma_\mu(E_{\nu_\mu})$ coincide with each other asymptotically. This is clearly demonstrated in the extreme relativistic limit (ERL) where $|\mathbf{p}_\ell|/E_\ell \to 1$, and the neutrino-nucleus cross sections depend on m_ℓ only through the threshold energy, as shown Appendix C here. Figure 4 in Ref. [74] is also illustrative in this respect.

Therefore, we focus our attention only on the QE cross section $\sigma_e(E_{\nu_e})$, as at the muon-neutrino energies involved in the MiniBooNE experiment [13], it is equal to $\sigma_\mu(E_{\nu_\mu})$ for all practical purposes.

One of the main objectives of the present study is to analyze the effect of the size of the configuration space up to neutrino energies of several hundred MeV. As in several previous works [34,39–44,48–52,54,57,68–70,74] this is done in first-order perturbation theory. The consequences of the particle-particle force in the $S = 1$, $T = 0$ channel, within the PQRPA, is also examined. The importance of this piece of the residual interaction was discovered more than 20 years ago by Vogel and Zirnbauer [75] and Cha [76], and since then the QRPA has become the most frequently used nuclear structure method for evaluating double β-decay rates.

A few words are devoted as well as to the nonrelativistic formalisms for neutrino-nucleus scattering. The most popular one was developed by the Walecka group [34,77–79], in which the nuclear transition matrix elements are classified as Coulomb, longitudinal, transverse electric, and transverse magnetic multipole moments. We feel that these denominations might be convenient when simultaneously discussing charge-conserving and charge-exchange processes, but it seems unnatural when one considers only the latter ones. As a matter of fact, this terminology is not often used in nuclear β-decay, μ-capture, and charge-exchange reactions, where one speaks only of vector and axial matrix elements with different degrees of forbiddenness: allowed (GT and Fermi), first forbidden, second forbidden, etc., types [80,81]. There are exceptions, of course, as, for instance, the recent work of Marketin *et al.* [52] on muon capture, where Walecka's classification was used.

The formalism worked out by Kuramoto *et al.* [74] is also frequently used for evaluation of neutrino-nucleus cross sections. It is simpler than that of Walecka, but it does not contain relativistic matrix elements, nor is it applicable for muon capture rates.

More recently, we have introduced another formalism [48–50]. Besides being almost as simple as that of Ref. [74], it retains relativistic terms and can be used for μ capture. This formalism is briefly sketched here, including the consequences of the violation of the conserved vector current (CVC) by the Coulomb field. It is further simplified by classifying the nuclear matrix elements in natural and unnatural parities. We also show how, within the present formalism, both the sum-rule approach and the formula for ERL look like.

In Sec. II we briefly describe the formalism used to evaluate different weakly interacting processes. Some details are delegated to the Appendixes: (A) contributions of natural and unnatural parity states to the transition rates, (B) the sum-rule approach for the inclusive neutrino-nucleus cross section, (C) the formula for the inclusive neutrino-nucleus cross section at the extreme relativistic limit, and (D) the formula for the muon-capture rate. In Sec. III we present and discuss the numerical results. Comparisons with experimental

[2]One should keep in mind that the mean lives of ^{12}N and ^{12}B are, respectively, 11.0 and 20.2 ms, while strong interaction times are of the order of 10^{-21} s.

data, as well as with previous theoretical studies, are done whenever possible. Here we first sketch the two theoretical frameworks, namely, the PQRPA and RQRPA, used in the numerical calculations. In Secs. II and III B we present the results for the exclusive and inclusive processes, respectively. Finally, in Sec. IV we give a brief summary and final conclusions.

II. FORMALISM FOR WEAKLY INTERACTING PROCESSES

The weak Hamiltonian is expressed in the form [77,78,82]

$$H_W(\mathbf{r}) = \frac{G}{\sqrt{2}} J_\alpha l_\alpha e^{-i\mathbf{r}\cdot\mathbf{k}}, \tag{2.1}$$

where $G = (3.045\,45 \pm 0.000\,06) \times 10^{-12}$ is the Fermi coupling constant (in natural units), the leptonic current $l_\alpha \equiv \{\mathbf{l}, il_\emptyset\}$ is given by Eq. (2.3) in Ref. [49], and the hadronic current operator $J_\alpha \equiv \{\mathbf{J}, iJ_\emptyset\}$, in its nonrelativistic form, reads[3]

$$\begin{aligned} J_\emptyset &= g_{\rm V} + (\overline{g}_{\rm A} + \overline{g}_{\rm P1})\boldsymbol{\sigma}\cdot\hat{\mathbf{k}} + g_A \frac{i\boldsymbol{\sigma}\cdot\boldsymbol{\nabla}}{\rm M}, \\ \mathbf{J} &= -g_{\rm A}\boldsymbol{\sigma} - i\overline{g}_{\rm W}\boldsymbol{\sigma}\times\hat{\mathbf{k}} - \overline{g}_{\rm V}\hat{\mathbf{k}} + \overline{g}_{\rm P2}(\boldsymbol{\sigma}\cdot\hat{\mathbf{k}})\hat{\mathbf{k}} - g_V\frac{i\boldsymbol{\nabla}}{\rm M}, \end{aligned} \tag{2.2}$$

where $\hat{\mathbf{k}} \equiv \mathbf{k}/|\mathbf{k}|$. The quantity

$$k = P_i - P_f \equiv \{\mathbf{k}, ik_\emptyset\} \tag{2.3}$$

is the momentum transfer, M is the nucleon mass, and P_i and P_f are momenta of the initial x and final nucleon (nucleus). The effective vector, axial-vector, weak-magnetism, and pseudoscalar dimensionless coupling constants are, respectively,

$$\begin{aligned} &g_V = 1, \quad g_A = 1, \quad g_M = \kappa_p - \kappa_n = 3.70, \\ &g_P = g_A \frac{2{\rm M}{\rm m}_\ell}{k^2 + {\rm m}_\pi^2}, \end{aligned} \tag{2.4}$$

where the following short notation has been introduced:

$$\begin{aligned} &\overline{g}_{\rm V} = g_{\rm V}\frac{\kappa}{2{\rm M}}, \quad \overline{g}_{\rm A} = g_{\rm A}\frac{\kappa}{2{\rm M}}, \quad \overline{g}_{\rm W} = (g_{\rm V} + g_{\rm M})\frac{\kappa}{2{\rm M}}, \\ &\overline{g}_{\rm P1} = g_{\rm P}\frac{\kappa}{2{\rm M}}\frac{k_\emptyset}{{\rm m}_\ell}, \quad \overline{g}_{\rm P2} = g_{\rm P}\frac{\kappa}{2{\rm M}}\frac{\kappa}{{\rm m}_\ell}, \end{aligned} \tag{2.5}$$

where $\kappa \equiv |\mathbf{k}|$. These estimates for g_M and g_P come from the CVC hypothesis and from the partially conserved axial vector current hypothesis, respectively. The finite nuclear size effect is incorporated via the dipole form factor with cutoff $\Lambda = 850$ MeV, that is, $g \to g[\Lambda^2/(\Lambda^2 + k^2)]^2$.

In performing the multipole expansion of the nuclear operators,

$$O_\alpha \equiv (\mathbf{O}, iO_\emptyset) = J_\alpha e^{-i\mathbf{k}\cdot\mathbf{r}}, \tag{2.6}$$

it is convenient (1) to take the momentum $\mathbf{k}$ along the z axis, that is,

$$\begin{aligned} e^{-i\mathbf{k}\cdot\mathbf{r}} &= \sum_{\rm L} i^{-{\rm L}}\sqrt{4\pi(2{\rm L}+1)}\, j_{\rm L}(\rho)Y_{{\rm L}0}(\hat{\mathbf{r}}), \\ &= \sum_{\rm J} i^{-{\rm J}}\sqrt{4\pi(2{\rm J}+1)}\, j_{\rm J}(\rho)Y_{{\rm J}0}(\hat{\mathbf{r}}), \end{aligned} \tag{2.7}$$

where $\rho = \kappa r$, and (2) to define the operators O_α as

$$O_\alpha = \sqrt{4\pi}\sum_{\rm J} i^{-{\rm J}}\sqrt{2{\rm J}+1}\,\mathsf{O}_{\alpha{\rm J}}. \tag{2.8}$$

In this way we avoid the troublesome factor $i^{-{\rm J}}$. In spherical coordinates ($m = -1, 0, +1$) we have

$$\begin{aligned} J_\emptyset &= g_{\rm V} + (\overline{g}_{\rm A} + \overline{g}_{\rm P1})\sigma_0 + ig_A{\rm M}^{-1}\boldsymbol{\sigma}\cdot\boldsymbol{\nabla}, \\ J_m &= -g_{\rm A}\sigma_m + m\overline{g}_{\rm W}\sigma_m + \delta_{m0}[-\overline{g}_{\rm V} + \overline{g}_{\rm P2}\sigma_0] - ig_V{\rm M}^{-1}\nabla_m \end{aligned} \tag{2.9}$$

and

$$\begin{aligned} \mathsf{O}_{\emptyset{\rm J}} &= j_{\rm J}(\rho)Y_{{\rm J}0}(\hat{\mathbf{r}})J_\emptyset, \\ \mathsf{O}_{m{\rm J}} &= \sum_{\rm L} i^{{\rm J}-{\rm L}}F_{{\rm L}{\rm J}m}\, j_{\rm L}(\rho)[Y_{\rm L}(\hat{\mathbf{r}})\otimes\mathbf{J}]_{\rm J}, \end{aligned} \tag{2.10}$$

where

$$\begin{aligned} F_{{\rm L}{\rm J}m} &\equiv (-)^{{\rm J}+m}\sqrt{2{\rm L}+1}\begin{pmatrix} {\rm L} & 1 & {\rm J} \\ 0 & -m & m \end{pmatrix} \\ &= (-)^{1+m}(1, -m{\rm J}m|{\rm L}0) \end{aligned} \tag{2.11}$$

is a Clebsch-Gordan coefficient.[4]

Explicitly, from Eq. (2.9),

$$\mathsf{O}_{\emptyset{\rm J}} = g_V\mathcal{M}^V_{\rm J} + ig_A\mathcal{M}^A_{\rm J} + i(\overline{g}_{\rm A} + \overline{g}_{\rm P1})\mathcal{M}^A_{0{\rm J}}, \tag{2.12}$$

$$\mathsf{O}_{m{\rm J}} = i(\delta_{m0}\overline{g}_{\rm P2} - g_{\rm A} + m\overline{g}_{\rm W})\mathcal{M}^A_{m{\rm J}} + g_V\mathcal{M}^V_{m{\rm J}} - \delta_{m0}\overline{g}_{\rm V}\mathcal{M}^V_{\rm J}. \tag{2.13}$$

The elementary operators are given by

$$\begin{aligned} \mathcal{M}^V_{\rm J} &= j_{\rm J}(\rho)Y_{\rm J}(\hat{\mathbf{r}}), \\ \mathcal{M}^A_{\rm J} &= {\rm M}^{-1}j_{\rm J}(\rho)Y_{\rm J}(\hat{\mathbf{r}})\,(\boldsymbol{\sigma}\cdot\boldsymbol{\nabla}) \end{aligned} \tag{2.14}$$

and

$$\begin{aligned} \mathcal{M}^A_{m{\rm J}} &= \sum_{{\rm L}\geqslant 0} i^{{\rm J}-{\rm L}-1}F_{{\rm L}{\rm J}m}\, j_{\rm L}(\rho)\,[Y_{\rm L}(\hat{\mathbf{r}})\otimes\boldsymbol{\sigma}]_{\rm J}\,, \\ \mathcal{M}^V_{m{\rm J}} &= {\rm M}^{-1}\sum_{{\rm L}\geqslant 0} i^{{\rm J}-{\rm L}-1}F_{{\rm L}{\rm J}m}\, j_{\rm L}(\rho)[Y_{\rm L}(\hat{\mathbf{r}})\otimes\boldsymbol{\nabla}]_{\rm J}. \end{aligned} \tag{2.15}$$

The CVC relates the vector-current pieces of operator (2.6) as (see Eqs. (10.45) and (9.7) in Ref. [81])

$$\mathbf{k}\cdot\mathbf{O}^V \equiv \kappa O^V_0 = \tilde{k}_\emptyset O^V_\emptyset, \tag{2.16}$$

[3] As in Ref. [49] we use Walecka's notation [78] with the Euclidean metric for quadrivectors and $\alpha = 1, 2, 3, 4$. The only difference is that we substitute his indices (0, 3) with our indices ($\emptyset$, 0), where we use the index $\emptyset$ for the temporal component and the index 0 for the third spherical component.

[4] Their values are

$$\begin{aligned} &F_{{\rm J}+1,{\rm J},0} = -\sqrt{\tfrac{{\rm J}+1}{2{\rm J}+1}}, \quad F_{{\rm J}-1,{\rm J},0} = \sqrt{\tfrac{\rm J}{2{\rm J}+1}}, \quad F_{{\rm J}+1,{\rm J},\pm1} = \sqrt{\tfrac{\rm J}{2({\rm J}+1)}}, \\ &F_{{\rm J},{\rm J}-1,\pm1} = \sqrt{\frac{{\rm J}+1}{2({\rm J}+1)}}, \quad F_{{\rm J},{\rm J},0} = 0, \quad F_{{\rm J},{\rm J},\pm1} = \mp\tfrac{1}{\sqrt{2}}. \end{aligned}$$

with

$$\tilde{k}_\emptyset \equiv k_\emptyset - S(\Delta E_{\rm Coul} - \Delta {\rm M}), \tag{2.17}$$

where

$$\Delta E_{\rm Coul} \cong \frac{6e^2 Z}{5R} \cong 1.45\ ZA^{-1/3}\ {\rm MeV}, \tag{2.18}$$

is the Coulomb energy difference between the initial and the final nuclei, $\Delta {\rm M} = {\rm M}_n - {\rm M}_p = 1.29$ MeV is the neutron-proton mass difference, and $S = \pm 1$ for neutrino and antineutrino scattering, respectively.

The consequence of the CVC relation (2.16) is the substitution

$$g_v \mathcal{M}^V_{0\mathsf{J}} - \overline{g}_{\rm V} \mathcal{M}^V_{\mathsf{J}} \to \frac{\tilde{k}_\emptyset}{\kappa} g_v \mathcal{M}^V_{\mathsf{J}}, \tag{2.19}$$

in (2.13), and $\mathsf{O}_{m\mathsf{J}}$ now reads

$$\begin{aligned}\mathsf{O}_{m\mathsf{J}} = {} & i(\delta_{m0}\overline{g}_{\rm P2} - g_{\rm A} + m\overline{g}_{\rm W})\mathcal{M}^A_{m\mathsf{J}} \\ & + |m| g_v \mathcal{M}^V_{m\mathsf{J}} + \delta_{m0}\frac{\tilde{k}_\emptyset}{\kappa} g_{\rm V} \mathcal{M}^V_{\mathsf{J}}.\end{aligned} \tag{2.20}$$

The second term in (2.17) comes from the violation of the CVC by the electromagnetic interaction. Although it is frequently employed in nuclear β decay, as far as we know, it has never been considered before in neutrino-nucleus scattering. $\Delta E_{\rm Coul}$ is equal to 3.8, 9.8, and 20.0 MeV for ^{12}C, ^{56}Fe, and ^{208}Pb, respectively, and therefore the term just mentioned could be quite significant, especially for heavy nuclei.

The transition amplitude for the neutrino-nucleus reaction at a fixed value of κ, from the initial state $|0^+\rangle$ in the (Z, N) nucleus to the nth final state $|\mathsf{J}^\pi_n\rangle$ in the $(Z \pm 1, N \mp 1)$ nucleus, reads

$$\mathcal{T}_{\mathsf{J}^\pi_n}(\kappa) \equiv \sum_{s_\ell, s_\nu} \left|\left\langle \mathsf{J}^\pi_n \right| H_W(\kappa) |0^+\rangle\right|^2. \tag{2.21}$$

The momentum transfer here is $k = p_\ell - q_\nu$, with $p_\ell \equiv \{\mathbf{p}_\ell, iE_\ell\}$and $q_\nu \equiv \{\mathbf{q}_\nu, iE_\nu\}$, and after some algebra [49], one gets

$$\begin{aligned}\mathcal{T}_{\mathsf{J}^\pi_n}(\kappa) = 4\pi G^2 \Bigg[& \sum_{\alpha=\emptyset,0,\pm1} \left|\left\langle \mathsf{J}^\pi_n \right| |\mathsf{O}_{\alpha\mathsf{J}}(\kappa)| |0^+\rangle\right|^2 \mathcal{L}_\alpha \\ & - 2\Re\left(\left\langle \mathsf{J}^\pi_n \right| |\mathsf{O}_{\emptyset\mathsf{J}}(\kappa)| |0^+\rangle \left\langle \mathsf{J}^\pi_n \right| |\mathsf{O}_{0\mathsf{J}}(\kappa)| |0^+\rangle^*\right)\mathcal{L}_{\emptyset 0}\Bigg],\end{aligned} \tag{2.22}$$

where

$$\begin{aligned}\mathcal{L}_\emptyset &= 1 + \frac{|\mathbf{p}_\ell|\cos\theta}{E_\ell}, \\ \mathcal{L}_0 &= 1 + \frac{2q_0 p_0}{E_\ell E_\nu} - \frac{|\mathbf{p}_\ell|\cos\theta}{E_\ell}, \\ \mathcal{L}_{\pm1} &= 1 - \frac{q_0 p_0}{E_\ell E_\nu} \pm \left(\frac{q_0}{E_\nu} - \frac{p_0}{E_\ell}\right) S, \\ \mathcal{L}_{\emptyset 0} &= \frac{q_0}{E_\nu} + \frac{p_0}{E_\ell}\end{aligned} \tag{2.23}$$

are the lepton traces, with $\theta \equiv \hat{\mathbf{q}}_\nu \cdot \hat{\mathbf{p}}_\ell$ being the angle between the incident neutrino and the ejected lepton momenta, and

$$\begin{aligned}q_0 &= \hat{k} \cdot \mathbf{q}_\nu = \frac{E_\nu(|\mathbf{p}_\ell|\cos\theta - E_\nu)}{\kappa}, \\ p_0 &= \hat{k} \cdot \mathbf{p}_\ell = \frac{|\mathbf{p}_\ell|(|\mathbf{p}_\ell| - E_\nu\cos\theta)}{\kappa}\end{aligned} \tag{2.24}$$

are the z components of the neutrino and lepton momenta.

The exclusive cross section (ECS) for the state $|\mathsf{J}^\pi_n\rangle$, as a function of the incident neutrino energy E_ν, is

$$\sigma_\ell(\mathsf{J}^\pi_n, E_\nu) = \frac{|\mathbf{p}_\ell| E_\ell}{2\pi} F(Z+S, E_\ell) \int_{-1}^{1} d(\cos\theta) \mathcal{T}_{\mathsf{J}^\pi_n}(\kappa), \tag{2.25}$$

where

$$\begin{aligned}E_\ell &= E_\nu - \omega_{\mathsf{J}^\pi_n},\ |\mathbf{p}_\ell| = \sqrt{\left(E_\nu - \omega_{\mathsf{J}^\pi_n}\right)^2 - m_\ell^2}, \\ \kappa &= |\mathbf{p}_\ell - \mathbf{q}_\nu| \\ &= \sqrt{2E_\nu(E_\ell - |\mathbf{p}_\ell|\cos\theta) - m_\ell^2 + \omega^2_{\mathsf{J}^\pi_n}},\end{aligned} \tag{2.26}$$

and $\omega_{\mathsf{J}^\pi_n} = -k_\emptyset = E_\nu - E_\ell$ is the excitation energy of the state $|\mathsf{J}^\pi_n\rangle$ relative to the state $|0^+\rangle$. Moreover, $F(Z+S, E_\ell)$ is the Fermi function for the neutrino ($S = 1$) and antineutrino ($S = -1$), respectively.

It is well known that charged-current cross sections must be corrected for the distortion of the outgoing lepton wave function by the Coulomb field of the daughter nucleus. For relatively low neutrino energies (∼40–50 MeV) this correction was implemented by numerical solution of the Dirac equation for an extended nuclear charge [81]. At higher energies, the effect of the Coulomb field was described by the effective momentum approximation (EMA) [83], in which the lepton momentum p_ℓ and energy E_ℓ are modified by the corresponding effective quantities (see Eqs. (34) and (45) in Ref. [51]).

Here, we also deal with the inclusive cross section (ICS),

$$\sigma_\ell(E_\nu) = \sum_{\mathsf{J}^\pi_n} \sigma_\ell\left(\mathsf{J}^\pi_n, E_\nu\right), \tag{2.27}$$

as well as with folded cross sections, both exclusive,

$$\overline{\sigma}_\ell\left(\mathsf{J}^\pi_n\right) = \int dE_\nu \sigma_\ell\left(\mathsf{J}^\pi_n, E_\nu\right) n_\ell(E_\nu), \tag{2.28}$$

and inclusive,

$$\overline{\sigma}_\ell = \int dE_\nu \sigma_\ell(E_\nu) n_\ell(E_\nu), \tag{2.29}$$

where $n_\ell(E_\nu)$ is the neutrino (antineutrino) normalized flux. In the evaluation of both neutrino and antineutrino ICSs the summation in Eq. (2.27) goes over all n states with spin and parity $\mathsf{J}^\pi \leqslant 7^\pm$ in the PQRPA and over $\mathsf{J}^\pi \leqslant 14^\pm$ in the RQRPA.

In Appendix A we show that the real and imaginary parts of the operators $\mathsf{O}_{\alpha\mathsf{J}}$, given by Eqs. (2.12) and (2.20), contribute to natural and unnatural parity states, respectively. This greatly simplifies the numerical calculations, because one always deals with real operators only. In Appendix D are also shown

the formula for the muon-capture process within the present formalism.

III. NUMERICAL RESULTS AND DISCUSSION

The major part of the numerical calculations was done within the PQRPA by employing the δ interaction (in MeV fm^3),

$$V = -4\pi(v_s P_s + v_t P_t)\,\delta(r),$$

with singlet (v_s) and triplet (v_t) coupling constants different for the particle-hole (ph), particle-particle (pp), and pairing (pair) channels [84]. This interaction leads to a good description of single and double β decays and it has been used extensively in the literature [85–88]. The s.p. wave functions were approximated with those of the harmonic oscillator (HO) with length parameter $b = 1.67$ fm, which corresponds to the oscillator energy $\hbar\omega = 45A^{-1/3} - 25A^{-2/3}$ MeV. The s.p. spaces S_2, S_3, S_4, and $S_6$are explored.

In Refs. [48] and [49], where the S_3 space was used, we pointed out that the values of the coupling strengths v_s^{pp}, $v_s^{\rm pair}$, and v_t^p used in $N > Z$ nuclei ($v_s^{pp} = v_s^{\rm pair}$, $v_t^{pp} \gtrsim v_s^{pp}$) might not be suitable for $N = Z$ nuclei. In fact, the best agreement with data in ^{12}C for (i) the energy of the ground state in ^{12}N, $E(^{12}\mathrm{N})$, (ii) the GT B values in ^{12}C, $B(^{12}\mathrm{N})$ and $B(^{12}\mathrm{B})$, and (iii) the exclusive muon capture in ^{12}B, $\Lambda^{\rm exc} \equiv \Lambda(1_1^+)$ is obtained when the pp channel is totally switched off, that is, $v_s^{pp} \equiv v_t^{pp} = 0$. The adopted ph coupling strengths are $v_s^{ph} = 27$ MeV fm^3 and $v_t^{ph} = 64$ MeV fm^3 [48]. For the pp channel it is convenient to define the parameters

$$s = \frac{v_s^{pp}}{v_s^{\rm pair}}, \quad t = \frac{v_t^{pp}}{v_s^{\rm pair}},$$

where $v_s^{\rm pair} = [v_s^{\rm pair}(p) + v_s^{\rm pair}(n)]/2$ [88]. As in our previous work on ^{12}C, here we use the same singlet and triplet pp couplings, that is, $s \equiv t$ [48,49]. States with $\mathrm{J}^\pi = 0^+$ and $\mathrm{J}^\pi = 1^+$ depend only on s and t, respectively, while all remaining states depend on both coupling strengths.

The s.p. energies and pairing strengths for S_2, S_3, and S_4 spaces were varied in a χ^2 search to account for the experimental spectra of odd-mass nuclei ^{11}C, ^{11}B, ^{13}C, and ^{13}N, as explained in Ref. [49]. This method, however, is not practical for space S_6, which comprises 21 s.p. levels. Therefore in this case the energies were derived in the manner used in Ref. [51], while the pairing strengths were adjusted to reproduce the experimental gaps in ^{12}C [89], considering all quasiparticle energies up to 100 MeV.

For the purpose of the present study, we also employ the RQRPA theoretical framework [90]. In this case the ground state is calculated in the relativistic Hartree-Bogoliubov model (RHB) using effective Lagrangians with density-dependent meson-nucleon couplings and DD-ME2 parameterization [91], and pairing correlations are described by the finite-range Gogny force [92]. Details of the formalism can be found in Refs. [93] and [94]. The RHB equations and respective equations for mesons are usually solved by expanding the Dirac spinors and the meson fields in a spherical HO basis with the S_{20} s.p. space. In the present study of neutrino-nucleus cross sections, with energies of incoming neutrinos up to 600 MeV, we extend the number of oscillator shells up to $N = 30$ to accommodate s.p. states at higher energies necessary for description of cross sections involving higher energies of incoming (anti)neutrinos. The number of $2qp$ configurations in the RQRPA is constrained by the maximal excitation energy E_{2qp}. Within the RHB + RQRPA framework the oscillator basis is used only in the RHB to determine the ground-state and s.p. spectra. The resulting wave functions are converted to coordinate space for evaluation of RQRPA matrix elements. However, it is the original HO basis employed in the RHB that determines the maximal E_{2qp} and the size of the RQRPA configuration space.

A. Weak interaction properties of ^{12}N and ^{12}B ground states

Let us first compare the QRPA and PQRPA within the smallest configuration space S_2, which contains 16 $\mathrm{J}^\pi = 1^+$ states, and with null pp coupling, $t = 0$. The PQRPA ground-state energies in ^{12}N and ^{12}B, are, respectively, $\omega_{+1}(1^+) = 18.319$ MeV and $\omega_{-1}(1^+) = 12.528$ MeV, while the corresponding wave functions read

$$\begin{aligned}|^{12}\mathrm{N}\rangle = {} & 0.963\left|1p^\pi_{3/2}1p^\nu_{1/2}\right\rangle + 0.232\left|1p^\pi_{3/2}1p^\nu_{3/2}\right\rangle \\ & + 0.122\left|1p^\pi_{1/2}1p^\nu_{3/2}\right\rangle + 0.105\left|1p^\pi_{1/2}1p^\nu_{1/2}\right\rangle \\ & + \ldots \end{aligned} \tag{3.1}$$

and

$$\begin{aligned}|^{12}\mathrm{B}\rangle = {} & -0.971\left|1p^\pi_{1/2}1p^\nu_{3/2}\right\rangle + 0.204\left|1p^\pi_{3/2}1p^\nu_{3/2}\right\rangle \\ & - 0.125\left|1p^\pi_{3/2}1p^\nu_{1/2}\right\rangle + 0.090\left|1p^\pi_{1/2}1p^\nu_{1/2}\right\rangle \\ & + \ldots . \end{aligned} \tag{3.2}$$

The analogous QRPA energies are quite similar: $\omega_{+1}(1^+) = 17.992$ MeV and $\omega_{-1}(1^+) = 12.437$ MeV. However, the wave functions are quite different. The main difference lies in the fact that QRPA furnishes the same wave functions for all four nuclei ^{12}N, ^{10}B, ^{14}N, and ^{12}B, being that of the ground state:

$$\begin{aligned}|1^+_{GS}\rangle = {} & -0.272\left|1p^\pi_{3/2}1p^\nu_{1/2}\right\rangle - 0.759\left|1p^\pi_{3/2}1p^\nu_{3/2}\right\rangle \\ & + 0.356\left|1p^\pi_{1/2}1p^\nu_{3/2}\right\rangle - 0.472\left|1p^\pi_{1/2}1p^\nu_{1/2}\right\rangle \\ & + \ldots . \end{aligned} \tag{3.3}$$

The difference in the wave functions is an important issue that clearly signals the need for number projection. In fact, the PQRPA yields the correct limits ($1p^\pi_{3/2} \to 1p^\nu_{1/2}$ and $1p^\nu_{3/2} \to 1p^\pi_{1/2}$) for one-particle-one-hole ($1p1h$) excitations on the ^{12}C ground state to reach the ^{12}N, and ^{12}B nuclei. All remaining configurations in Eqs. (3.1) and (3.2) come from the higher order $2p2h$ and $3p3h$ excitations. On the contrary, the QRPA state, Eq. (3.3), is dominantly the two-hole excitation $[(1p^\pi_{3/2})^{-1}, (1p^\nu_{3/2})^{-1}]$, which corresponds to the ground state of ^{10}B. More details on this question can be found in Fig. 3 of Ref. [49]. The 1p1h amplitudes $[(1p^\pi_{3/2})^{-1}, 1p^\nu_{1/2}]$ and $[(1p^\nu_{3/2})^{-1}, (1p^\pi_{1/2})]$ are dominantly present in the following

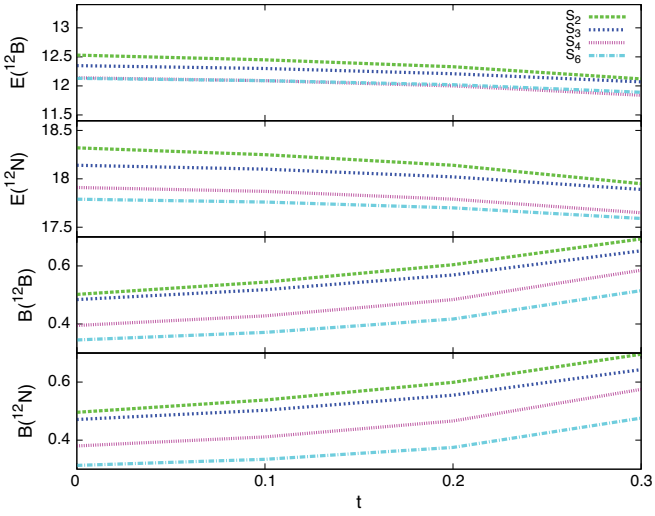

FIG. 1. (Color online) ^{12}B and ^{12}N ground-state energies (in units of MeV) and GT B values within the PQRPA for different s.p. spaces, as a function of the pp-coupling t. Experimental values are $E(^{12}\mathrm{B}) = 13.37$ MeV and $E(^{12}\mathrm{N}) = 17.33$ MeV [95], and $B(^{12}\mathrm{B}) = 0.466$, and $B(^{12}\mathrm{N}) = 0.526$ [96].

QRPA states:

$$
\begin{aligned}
|1_2^+\rangle &= 0.708\left|1p^{\pi}_{1/2}1p^{\nu}_{3/2}\right\rangle + 0.703\left|1p^{\pi}_{3/2}1p^{\nu}_{1/2}\right\rangle \\
&\quad + \cdots \\
|1_4^+\rangle &= -0.476\left|1p^{\pi}_{3/2}1p^{\nu}_{1/2}\right\rangle + 0.437\left|1p^{\pi}_{3/2}1p^{\nu}_{3/2}\right\rangle \\
&\quad + 0.441\left|1p^{\pi}_{1/2}1p^{\nu}_{3/2}\right\rangle - 0.096\left|1p^{\pi}_{1/2}1p^{\nu}_{1/2}\right\rangle \\
&\quad + \cdots . \qquad (3.4)
\end{aligned}
$$

The wave functions in Eq. (3.4) clearly demonstrate the superiority of the PQRPA to the QRPA. Therefore henceforth only the PQRPA results are discussed for the exclusive observables.

Figure 1 shows the ^{12}B and ^{12}N ground-state energies, and the corresponding GT B values within the PQRPA for different s.p. spaces, as a function of the pp-coupling t. One sees that the energies depend rather weakly on both and agree fairly well with the measured energies, $E(^{12}\mathrm{B}) = 13.37$ MeV and $E(^{12}\mathrm{N}) = 17.33$ MeV [95], although the first one is somewhat underestimated, while the second one is somewhat overestimated. Both GT B values increase significantly with t and diminish when the size of the s.p. space is increased. For spaces S_2 and S_3 the best overall agreement with data ($B(^{12}\mathrm{B}) = 0.466$ and $B(^{12}\mathrm{N}) = 0.526$ [96]) is achieved with $t = 0$, while for spaces S_4 and S_6 this happens when the couplings are, respectively, $t = 0.2$ and $t = 0.3$.

After establishing the PQRPA parametrization, we analyze the behavior of the ECSs of the ground states in ^{12}N and ^{12}B, as a function of the size of the configuration space. Figure 2 shows the ECSs for the reaction $^{12}\mathrm{C}(\nu, e^-)^{12}\mathrm{N}$ (in units of 10^{-42} cm^2) for several configuration spaces, and for $t = 0$, within three energy intervals. The top panel represents the DAR region, where experimental data are available [25] and the search for neutrino oscillations was done [25,27]. The middle panel in Fig. 2 represents the region of interest

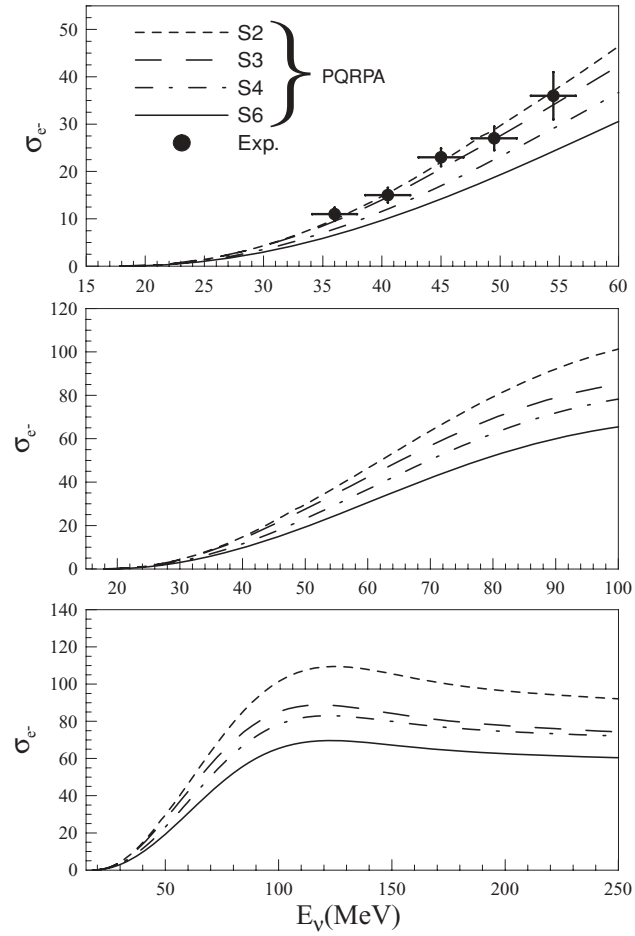

FIG. 2. Exclusive $^{12}\mathrm{C}(\nu, e^-)^{12}\mathrm{N}$ cross section $\sigma_e(E_\nu, 1_1^+)$ (in units of 10^{-42} cm^2), plotted as a function of the incident neutrino energy E_ν. Results for several single-particle spaces S_N, and $t = 0$, within three energy intervals, are shown. Experimental data in the DAR region are from Ref. [25].

for supernova neutrinos, as pointed out in Refs. [15] and [97], while the bottom panel shows the asymptotic behavior of the cross section, which becomes almost constant for $E_\nu \simeq 200$ MeV. Within the spaces S_2 and S_3 the calculations reproduce quite well the experimental cross sections in the DAR region, as shown in the first panel.

Figure 3 shows the calculated ECSs for the reaction $^{12}\mathrm{C}(\nu, e^-)^{12}\mathrm{N}$ within several configuration spaces, but now with different values of the pp coupling. From comparison with the experimental data in the DAR region [25], one observes that the appropriate values for the coupling t for s.p. spaces S_4, and S_6, are, respectively, $t = 0.2$ and $t = 0.3$, that is, the same as those required to reproduce the experimental energies and the GR B values in ^{12}B, and ^{12}N.

This change of parametrization hints at the self-consistency of the PQRPA and comes from the fact that, in this model, (i) the GT strength allocated in the ground state is moved to another 1^+ states when the size of the space is increased, and (ii) the effect of the pp residual interaction goes in the oppositive direction, returning the GT strength to the 1_1^+ state. Only for space S_2 is the cross section $\sigma_{e^-}(E_\nu, 1_1^+)$ appreciably

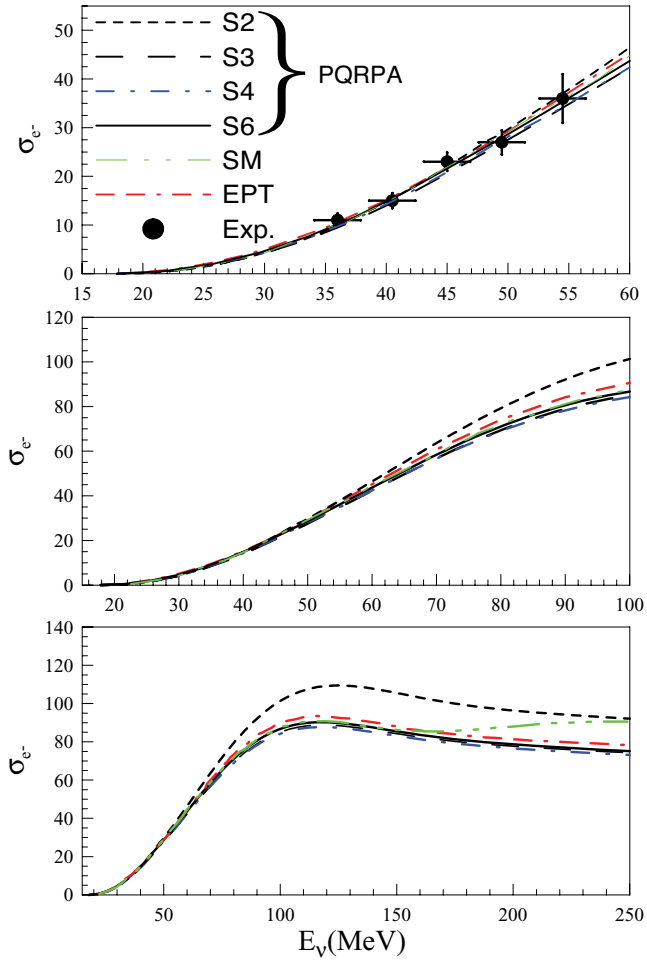

FIG. 3. (Color online) Same as Fig. 2, but here $t = 0$ for S_2 and S_3, $t = 0.2$ for S_4, and $t = 0.3$ for S_6. SM and EPT calculations are, respectively, from Refs. [98] and [16]. Experimental data in the DAR region are from Ref. [25].

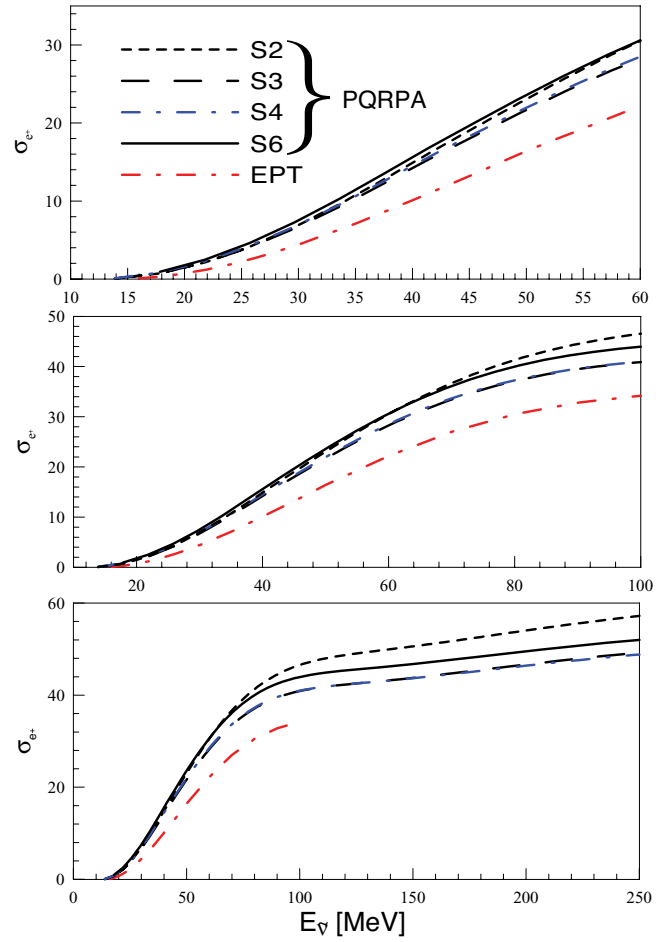

FIG. 4. (Color online) Calculated ^{12}C($\bar\nu, e^+$)^{12}B cross section $\sigma_{e^+}(E_{\bar\nu}, 1^+_1)$ (in units of 10^{-42} cm^2), plotted as a function of the incident antineutrino energy $E_{\bar\nu}$. As in Fig. 3, the value of t is 0 for s.p. spaces S_2, and S_3, 0.2 for S_4, and 0.3 for S_6. The EPT calculation from Ref. [16] is also shown.

larger (at $E_\nu \gtrsim 60$ MeV) than for the other spaces, which is just because of the small number of configurations in this case. Figure 3 also shows the results for the ECSs evaluated within the SM [98] and the EPT [16]. Both of them agree well with the data and with the present calculation.

The results for the reaction $(\bar\nu, e^+)$ to the ground state in ^{12}B are shown in Fig. 4. The cross section $\sigma_{e^+}(E_{\bar\nu}, 1^+_1)$ is similar to that produced by neutrinos but significantly smaller in magnitude. One notices that they are considerably different from the EPT results [16], which are also shown in Fig. 4. To some extent this is surprising, as in the case of neutrinos the two models yield very similar results. One should remember that in the EPT model the axial form factor, used for both neutrinos and antineutrinos, is gauged to the average of the GR B values in ^{12}B and ^{12}N, which, in turn, are well reproduced by the PQRPA. Therefore it is difficult to understand why the EPT results agree with the present calculations for neutrinos and disagree for antineutrinos.

Figure 5 shows the dependence on the configuration space of the exclusive muon-capture transition rate $\Lambda(1^+_1)$ to the ^{12}B ground state, and the electron and muon flux-averaged ECSs, given by Eq. (2.28), to the ^{12}N ground state, that is, $\overline{\sigma}_\epsilon(1^+_1)$ and $\overline{\sigma}_\mu(1^+_1)$. As in Refs. [48] and [49] the electron neutrino distribution $n_e(E_\nu)$ was approximated with the Michel energy spectrum [9,99], and for the muon neutrinos we used $n_\mu(E_\nu)$ from Ref. [30]. The energy integration is carried out in the DAR interval $m_e + \omega_{J_f} \leqslant \Delta^{\rm DAR}_{J_f} \leqslant 52.8$ MeV for electrons and in the DIF interval $m_\mu + \omega_{J_f} \leqslant \Delta^{\rm DIF}_{J_f} \leqslant 300$ MeV for muons. From Fig. 5 and comparison with experimental data,

$$\Lambda(^{12}\mathrm{B}) = 6.2 \pm 0.3 \text{ [45]},$$
$$\overline{\sigma}_e(^{12}\mathrm{N}) = 9.1 \pm 0.4 \pm 0.9 \text{ [25]}, \quad 8.9 \pm 0.3 \pm 0.9 \text{ [26]},$$
$$\overline{\sigma}_\mu(^{12}\mathrm{N}) = 6.6 \pm 1.0 \pm 1.0 \text{ [28]}, \quad 5.6 \pm 0.8 \pm 1.0 \text{ [29]},$$

one finds out, as for the results shown in Figs. 1 and 3, the model self-consistency between s.p. spaces and the pp couplings. That is, for larger s.p. spaces, larger values of t are required. In brief, the experimental data for $\overline{\sigma}_e(^{12}\mathrm{N})$ and $\overline{\sigma}_\mu(^{12}\mathrm{N})$ are well reproduced by the PQRPA. The same is true for the SM calculations [42,43], while in the RPA and QRPA models they are strongly overestimated, as shown in Table II in Ref. [43] and Table I in Ref. [50].

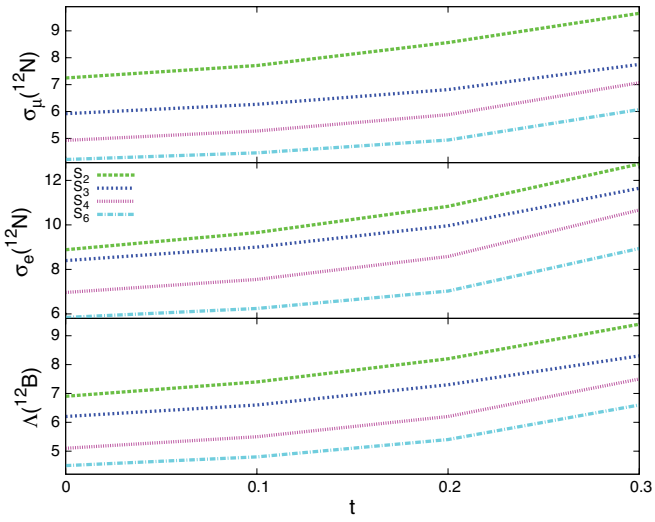

FIG. 5. (Color online) Muon-capture transition rate to the ^{12}B ground state (in units of 10^2 s^{-1}, and electron and muon folded ECSs to the ^{12}N ground state in units of 10^{-42} cm^2 and 10^{-41} cm^2, respectively. Experimental values, in these units, are $\Lambda(^{12}\mathrm{B}) = 6.2 \pm 0.3$ [45], $\overline{\sigma}_e(^{12}\mathrm{N}) = 9.1 \pm 0.4 \pm 0.9$ [25], and $\overline{\sigma}_e(^{12}\mathrm{N}) = 8.9 \pm 0.3 \pm 0.9$ [26] and $\overline{\sigma}_\mu(^{12}\mathrm{N}) = 6.6 \pm 1.0 \pm 1.0$ [28], and $\overline{\sigma}_\mu(^{12}\mathrm{N}) = 5.6 \pm 0.8 \pm 1.0$ [29], respectively.

B. Inclusive cross sections ^{12}C(ν, e^-)^{12}N and ^{12}C($\tilde{\nu}$, e^+)^{12}B and the Sum Rule

In Fig. 6 we compare the PQRPA results for the ICS $\sigma_{e^-}(E_\nu)$ within spaces S_2, S_3, and S_6 with the corresponding sum rules $\sigma_{e^-}^{SR}(E_\nu)$ evaluated from Eq. (B1). One immediately sees that the PQRPA results depend very strongly on the size of the employed s.p. space. In contrast, as mentioned in Appendix B, the sum rule $\sigma_{e^-}^{SR}(E_\nu)$ depends on the average energy $\overline{\omega_{J_n^\pi}}$. Here we use two values: $\overline{\omega_{J_n^\pi}} = 17.34$ MeV, which is the ground-state energy ^{12}N (GT resonance); and $\overline{\omega_{J_n^\pi}} = 42$ MeV, which is roughly the energy of the first forbidden resonance [100]. The corresponding curves in Fig. 6 are labeled, respectively, $\mathrm{SR_{GT}}$ and $\mathrm{SR_{1F}}$.

They should be the upper limits for allowed and first forbidden transitions, respectively. The validity of these sum rules is questionable for neutrinos energies of several hundred MeV, as pointed out by Kuramoto *et al.* [74]. In fact, we note that the cross section $\mathrm{SR_{GT}}$ ($\mathrm{SR_{1F}}$) exceeds the free particle cross section $\sigma_6 \equiv 6(\nu_e + n \to e^- + p)$ for $E_\nu > 200$ MeV ($E_\nu > 300$ MeV) [101].

Several previous SM and RPA-like calculations of $\sigma_{e^-}(E_\nu)$, employing different effective axial-vector coupling constants and different s.p. spaces, are exhibited in Fig. 6 as well, namely:

(i) the TDA [34], with $g_A = 1.23$, and S_2;
(ii) the SM and RPA [43], with $g_A = 0.88$, and S_3;
(iii) the CRPA [102], with $g_A = 1.26$, and S_4; and
(iv) RQRPA [51], with $g_A = 1.23$, S_{20}, and $E_{2qp} = 100$ MeV.

It is important to specify the g_A values because the partial cross sections are predominantly of the axial-vector type (especially the allowed ones), which are proportional to g_A^2. Despite the very significant differences in g_A and the

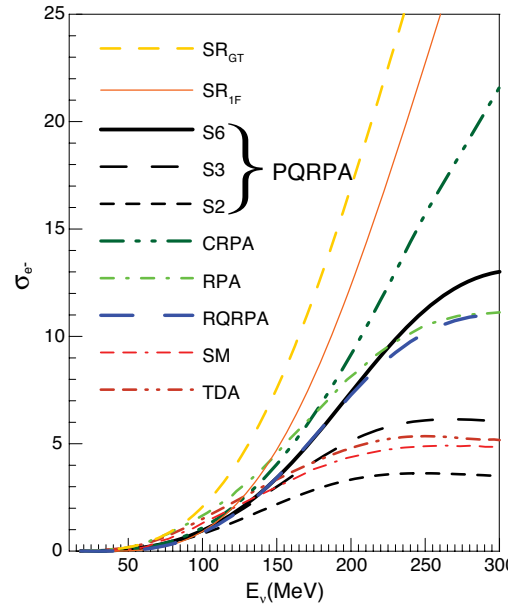

FIG. 6. (Color online) Inclusive ^{12}C(ν, e^-)^{12}N cross section $\sigma_{e^-}(E_\nu)$ (in units of 10^{-39} cm^2) plotted as a function of the incident neutrino energy E_ν. PQRPA results within s.p. spaces S_2, S_3, and S_6, and with the same values of $s = t$ as in Fig. 3, are compared with two sum-rule limits (as explained in the text), $\mathrm{SR_{GT}}$ and $\mathrm{SR_{1F}}$, obtained with an average excitation energy $\overline{\omega_{J_n^\pi}}$ of 17.34 and 42 MeV, respectively. Several previous RPA-like calculations, namely, the RPA [43], CRPA [102], and RQRPA within S_{20} for $E_{2qp} = 100$ MeV [51], as well as the SM [43] and the TDA [34], are also shown.

s.p. spaces, the different calculations of $\sigma_{e^-}(E_\nu)$ yield quite similar results for energies $E_\nu \lesssim 130$ MeV, lying basically in the vicinity of the sum-rule result $\mathrm{SR_{1F}}$. But for higher energies they could become quite different, and they are clearly separated in two groups at $E_\nu = 300$ MeV. In the first group, with $\sigma_{e^-}(E_\nu) \lesssim 5 \times 10^{-39}$ cm^2, are the SM, TDA, and PQRPA within spaces S_2 and S_3, while in the second group, with $\sigma_{e^-}(E_\nu) \gtrsim 10 \times 10^{-39}$ cm^2, are the RPA, RQRPA, CRPA, and PQRPA within space S_6. Volpe *et al.* [43] found that the difference between their SM and their RPA calculations was caused by differences in the correlations taken into account and to the too small SM space. We also note that only the CRPA result approaches the sum-rule limits for $E_\nu > 200$ MeV.

Similar results for the ^{12}C($\tilde{\nu}$, e^+)^{12}B ICS $\sigma_{e^+}(E_{\tilde{\nu}})$ are displayed in Fig. 7, and analogous comments can be made here. For comparison, we show the antineutrino-^{12}C cross-sections evaluated with the CRPA [102].

C. Large configuration spaces

As there are no experimental data on flux unfolded ICSs for $E_\nu \leqslant 400$ MeV, we cannot conclude which of the results displayed in Figs. 6 and 7 are good and which are not. We can only conclude that the ICSs strongly depend on the size of the s.p. space. In PQRPA calculations we are not able to use spaces lager than S_6 because of numerical difficulties. Thus instead of using the PQRPA, henceforth we employ the RQRPA, where such calculations are feasible. It is important to note that within

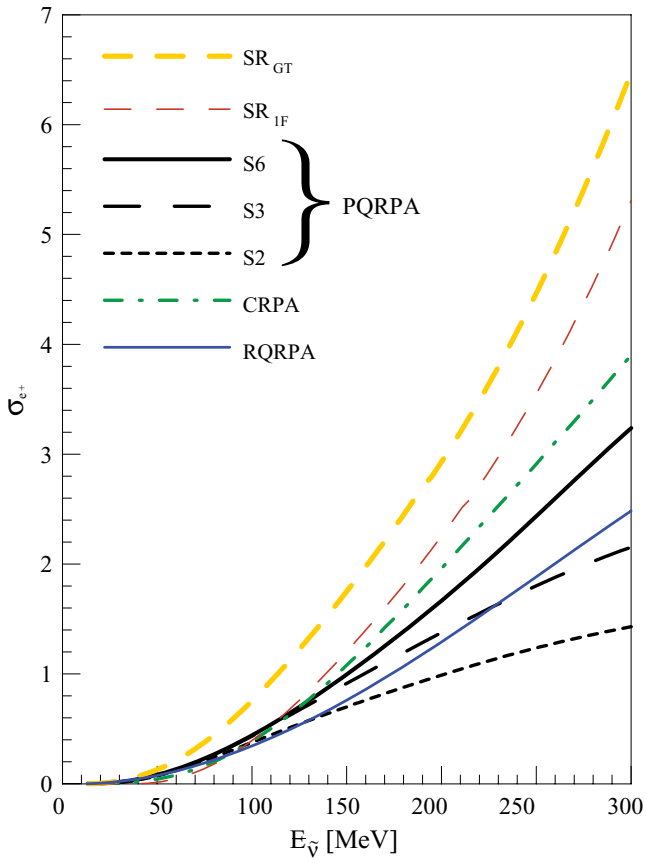

FIG. 7. (Color online) Inclusive ^{12}C($\tilde{\nu}, e^+$)^{12}B cross section $\sigma_{e^+}(E_{\nu})$ (in units of 10^{-39} cm^2) plotted as a function of the incident neutrino energy $E_{\tilde{\nu}}$. All results were obtained in the same way as in the neutrino case in Fig. 6.

the RHB + RQRPA model the oscillator basis is used only in the RHB calculation in order to determine the ground state and the s.p. spectra. The wave functions employed in RPA equations are obtained by converting the original HO basis to the coordinate representation. Therefore, the size of the RQRPA configuration space and $2qp$ energy cutoffs are determined by the number of oscillator shells in the RHB model.

First, we analyze the effect of the cutoff energy within the S_{20} space on $\sigma_{e^-}(E_{\nu})$ for E_{ν} up to 600 MeV. The left panel in Fig. 8 shows that at high energies this cross section increases roughly by a factor of 2 when E_{2qp} is augmented from 100 to 200 MeV. The increase in the cross section is also quite important when E_{2qp} is moved from 200 to 300 MeV. For the limiting value of $E_{2qp} = 300$ MeV, all possible configurations are included in RQRPA calculations. Next, we do the same within the S_{30} space, and the resulting $\sigma_{e^-}(E_{\nu})$ values are displayed in the right panel in Fig. 8. By comparing the two panels it is easy to see that up to $E_{2qp} = 300$ MeV the cross sections obtained with the S_{30} space are basically the same as those calculated with the S_{20} space. Small differences in the cross sections obtained using the S_{20} versus the S_{30} space for E_{2qp} up to 300 MeV are caused by modifications of positive-energy s.p. states contributing to the RQRPA configuration space within the restricted $2qp$ energy window. But for $E_{\nu} \gtrsim 400$ MeV additional transition strength appears in the S_{30} space when E_{2qp} is moved up to 400 MeV, after which further increase in E_{2qp} has a very small effect. We conclude therefore that the configuration space engendered by $N = 20$ HO shells with $E_{2qp} = 300$ MeV is large enough to describe $\sigma_{e^-}(E_{\nu})$ with E_{ν} up to 400 MeV. Similarly, the space brought about by $N = 30$ HO shells with $E_{2qp} = 400$ MeV is appropriate to account for $\sigma_{e^-}(E_{\nu})$ up to $E_{\nu} = 600$ MeV. For higher neutrino energies very likely we would have to continue increasing the number of shells.

Analogous results for antineutrino ICSs $\sigma_{e^+}(E_{\tilde{\nu}})$ are displayed in Fig. 9. One notes important differences in comparison with $\sigma_{e^-}(E_{\nu})$ results shown in Fig. 8. First, here the spaces S_{20} and S_{30} yield almost-identical results in the entire interval of antineutrino energies up to $E_{\tilde{\nu}} = 600$ MeV. Second, the successive increase in the cross sections when the cutoff E_{2qp} is augmented in steps of 100 MeV is smaller and decreases more rapidly than in the neutrino case. This suggests that the configuration space is now sufficiently large to appropriately account for $\sigma_{e^+}(E_{\tilde{\nu}})$ even at antineutrino energies higher than 600 MeV.

At present, owing to numerical difficulties, we cannot perform RQRPA calculations for the full range of neutrino energies where the QE cross section was measured at MiniBooNE [13], but only up to 0.6 GeV. However, we feel that this is still illustrative for comparison with data. This is done in Fig. 10, which is basically the portion of Fig. 21 in Ref. [73] for the QE $\sigma_{\mu^-}(E_{\nu})$ (see also Ref. [103]), with our result for $\sigma_{e^-}(E_{\nu})$ from Fig. 8 for S_{30} and $E_{2qp} =$ 500 MeV incorporated. As pointed out in the Introduction, at relatively high energies ($E_{\nu} > 300$ MeV) the electron and muon neutrino cross sections converge to each other, and therefore, in the present analysis, the electron neutrino cross section provides a reasonable upper limit estimate. One sees that we underestimate the data by almost a factor of 2. But one should keep in mind that, while we use $g_A = 1$ [see Eq. (2.4)], in the RFGM calculation done by Martini *et al.* [73,103], $g_A = 1.255$ was used. The axial-vector contribution being dominant for the latter value of the coupling constant, one would have to renormalize our $\sigma_{e^-}(E_{\nu})$ by a factor of $\sim$1.5. Such a result is also shown in Fig. 10, and although the resulting cross section still underestimates somewhat the data for $\sigma_{\mu^-}(E_{\nu})$, it is notably superior to the pure 1p-1h result from Ref. [73], where good agreement with the data is achieved only after considering additional two-body (2p-2h) and three-body (3p3h) decay channels. One should keep in mind, however, that as the weak decay Hamiltonian is a one-body operator, these excitations are only feasible via the ground-state correlations (GSCs), which basically redistribute the 1p-1h transition strength without increasing its total magnitude when the initial wave function is properly normalized. In the present work, as well as in all SM-like calculations, the GSC and a normalized initial-state wave function are certainly considered to all orders in perturbation theory, through the full diagonalization of the Hamiltonian matrix. In contrast, in Refs. [73] and [103] the GSCs are taken into account in second-order perturbation theory, but there are no references to the normalization of the ^{12}C ground-state wave function. How to carry out the normalization in the framework of the infinite nuclear matter model is discussed in a recent paper related to the

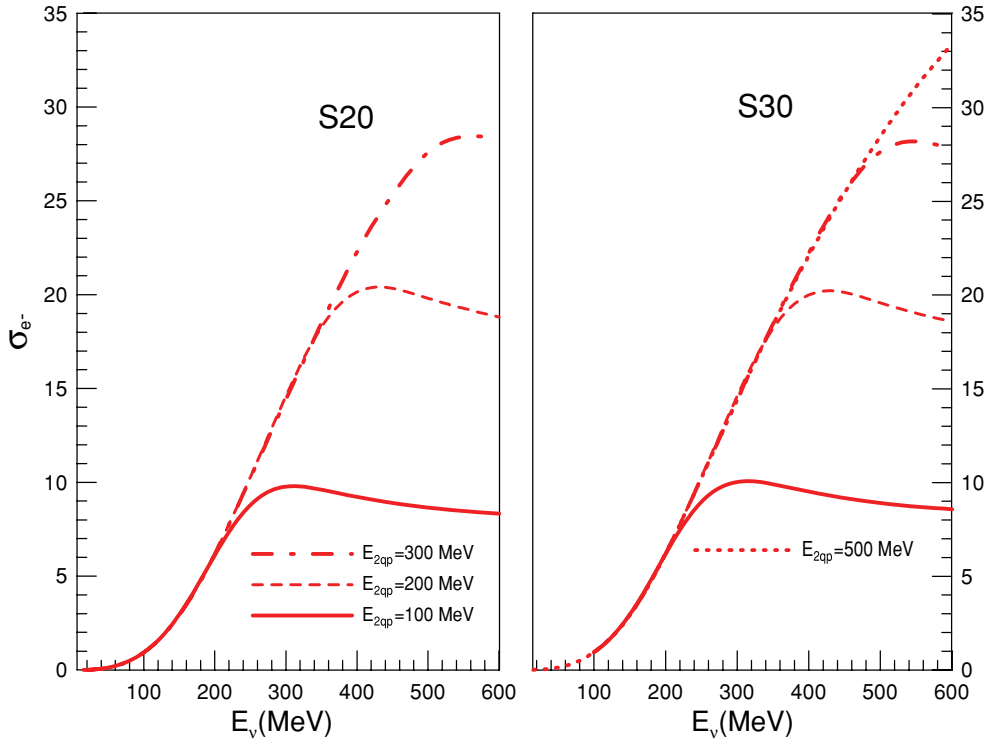

FIG. 8. (Color online) Inclusive ^{12}C(ν, e^-)^{12}N cross-section $\sigma_{e^-}(E_\nu)$(in units of 10^{-39} cm^2) plotted as a function of the incident neutrino energy E_ν, evaluated in RQRPA with different configuration spaces. These cross sections are plotted as functions of the incident neutrino energy with different cut-off of the E_{2qp} quasiparticle energy as it is explained in the text. The left and right panels show the cross section evaluated with S_{20}, and S_{30} s.p. spaces. The last cross section shows that the convergence of the calculation is achieved up to 600 MeV of incident neutrino energy.

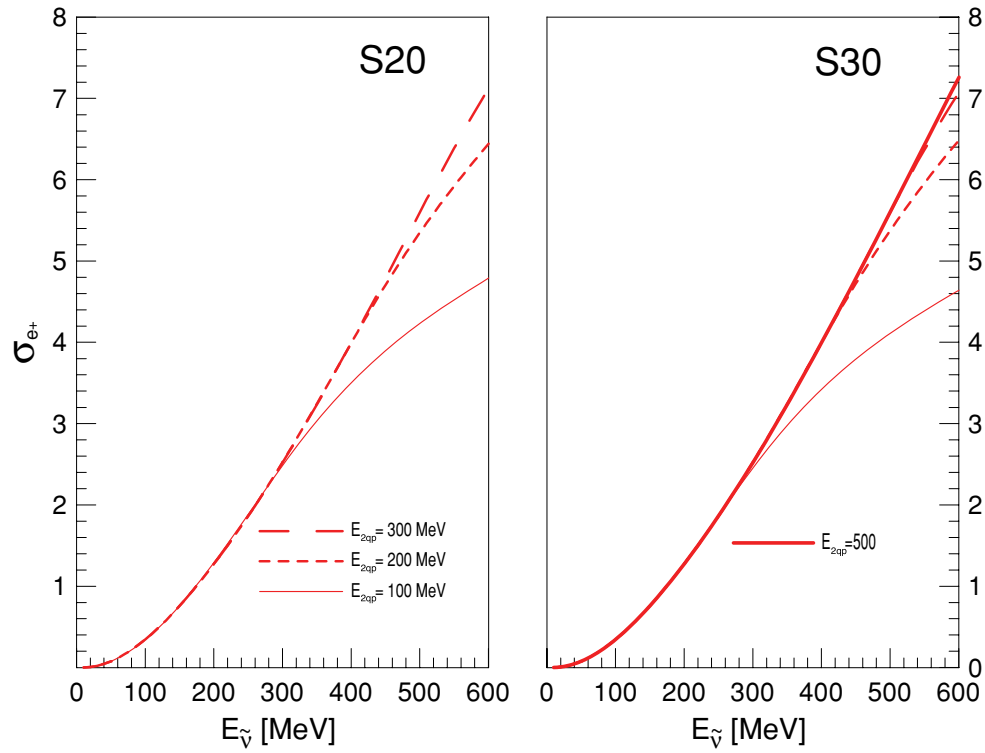

FIG. 9. (Color online) Same as Fig. 8 but for the ^{12}C($\tilde{\nu}$, e^+)^{12}B cross section $\sigma_{e^+}(E_{\tilde{\nu}})$.

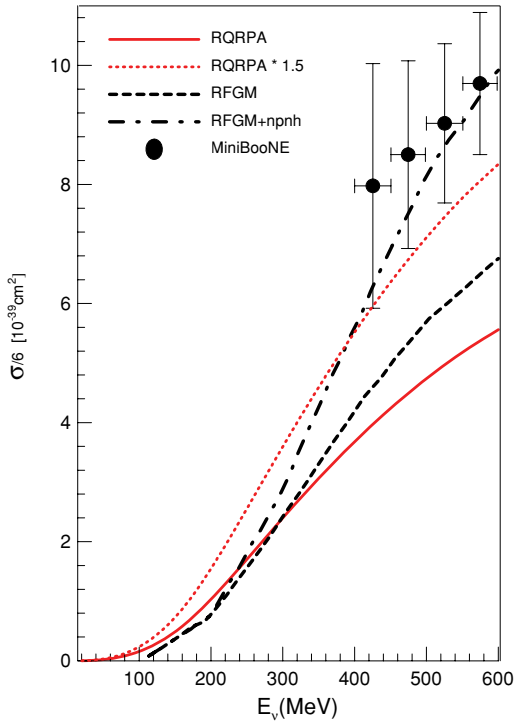

FIG. 10. (Color online) The calculated RQRPA (within S_{30} and $E_{2qp} = 500$ MeV) quasielastic $(\nu_e, {}^{12}\mathrm{C})$ cross section per neutron (solid line) is compared with that for the $(\nu_\mu, {}^{12}\mathrm{C})$ scattering data measured at MiniBooNE [13]; the dotted line shows the same calculation but renormalized by a factor of 1.5. Also displayed are the calculations done by Martini *et al.* [73,103] within the RFGM for pure (1p-1h) excitations (dashed line) and with the inclusion of the np-nh channels (dot-dashed line).

nonmesonic weak decay of the hypernucleus ${}^{12}_{\Lambda}\mathrm{C}$ [104]; see also Refs. [105–107].

D. Multipole decomposition of cross sections

We have not yet mentioned the contributions of different multipoles to the ICSs. Normally, the RHB model within S_{20}, and with $\mathrm{J}^\pi \leqslant 7^\pm$, provides converged results for RQRPA excitation spectra at incident neutrino energies $E_\nu \leqslant 300$ MeV, as shown in Fig. 2 of Ref. [51]. But this is not the case for neutrino-nucleus cross sections at energies $E_\nu \gtrsim 300$ MeV, where one has to consider high cutoff energies E_{2qp}. In fact, it is necessary to consider more and more multipoles as the configuration space is enlarged by increasing E_{2qp}. This is illustrated in Fig. 11 for the case of $E_{2qp} = 500$ MeV. One sees that all multipoles are significant up to $\mathrm{J}^\pi = 14^\pm$ for neutrinos and up to $\mathrm{J}^\pi = 11^\pm$ for antineutrinos.

Next we discuss partial multipole contributions to the ICS, with a focus on the degree of forbiddenness of the transition matrix elements, for the following cross sections.

(i) Allowed: $\sigma^A_{e^+}(E_{\tilde\nu})$, with $\mathrm{J}^\pi = 0^+, 1^+$.
(ii) First forbidden: $\sigma^{1F}_{e^+}(E_{\tilde\nu})$, with $\mathrm{J}^\pi = 0^-, 1^-, 2^-$.
(iii) Second forbidden: $\sigma^{2F}_{e^+}(E_{\tilde\nu})$, with $\mathrm{J}^\pi = 2^+, 3^+$.
(iv) Third forbidden $\sigma^{3F}_{e^+}(E_{\tilde\nu})$ with $\mathrm{J}^\pi = 3^-, 4^-$.

Thus, in the left panel in Fig. 12 we show these individual contributions for the inclusive ${}^{12}\mathrm{C}(\tilde\nu, e^+){}^{12}\mathrm{B}$ cross section $\sigma_{e^+}(E_{\tilde\nu})$, evaluated within both the PQRPA (spaces S_2 and S_6) the RQRPA (space S_{30} with $E_{2qp} = 500$ MeV).

The same is done for the corresponding derivatives, that is, the spectral functions $d\sigma_{e^+}(E_{\tilde\nu})/dE_{\tilde\nu}$, in the right panel in Fig. 12. Several conclusions can be drawn. First, as in the case of total $\sigma_{e^+}(E_{\tilde\nu})$, they depend very strongly on the size of the configuration space. This dependence, in turn, increases with the degree of forbiddenness; that is, it is more pronounced for first-forbidden than for allowed transitions, and so on. Second, within the PQRPA the allowed cross section $\sigma^A_{e^+}(E_{\tilde\nu})$ exhibits a resonant pattern at low energy, and is dominant for $E_{\tilde\nu} \lesssim 50$ MeV. For large s.p. spaces its contribution is

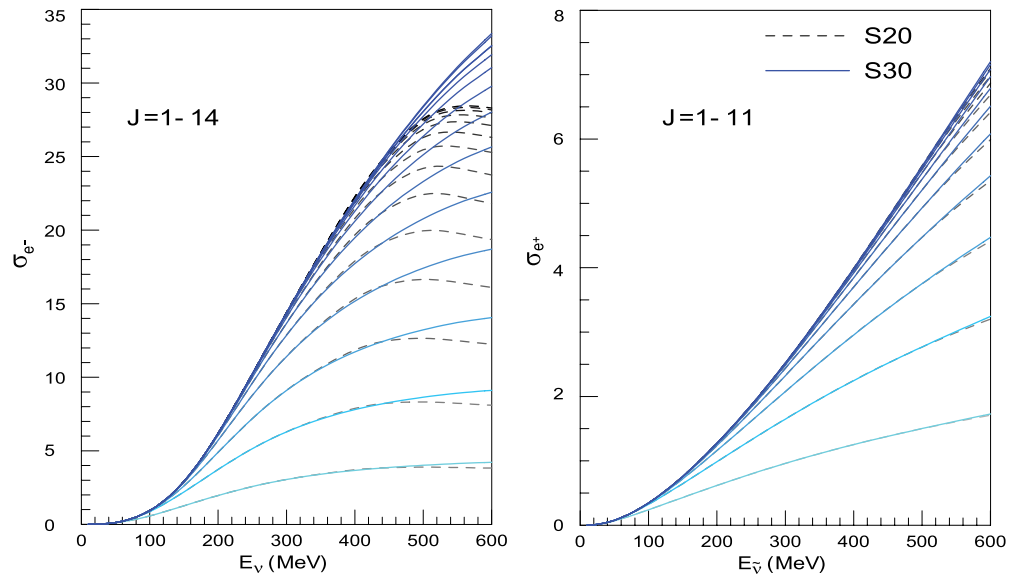

FIG. 11. (Color online) Left and right panels show, respectively, the cross sections $\sigma_{e^-}(E_\nu)$, and $\sigma_{e^+}(E_{\tilde\nu})$ (in units of 10^{-39} cm^2) evaluated in RQRPA for S_{20}, and S_{30} s.p. spaces with the cutoff $E_{2qp} = 500$ MeV, and different maximal values of $\mathrm{J}^\pm$, with J going from 1 up to 14 for neutrinos, and from 1 up to 11 for antineutrinos.

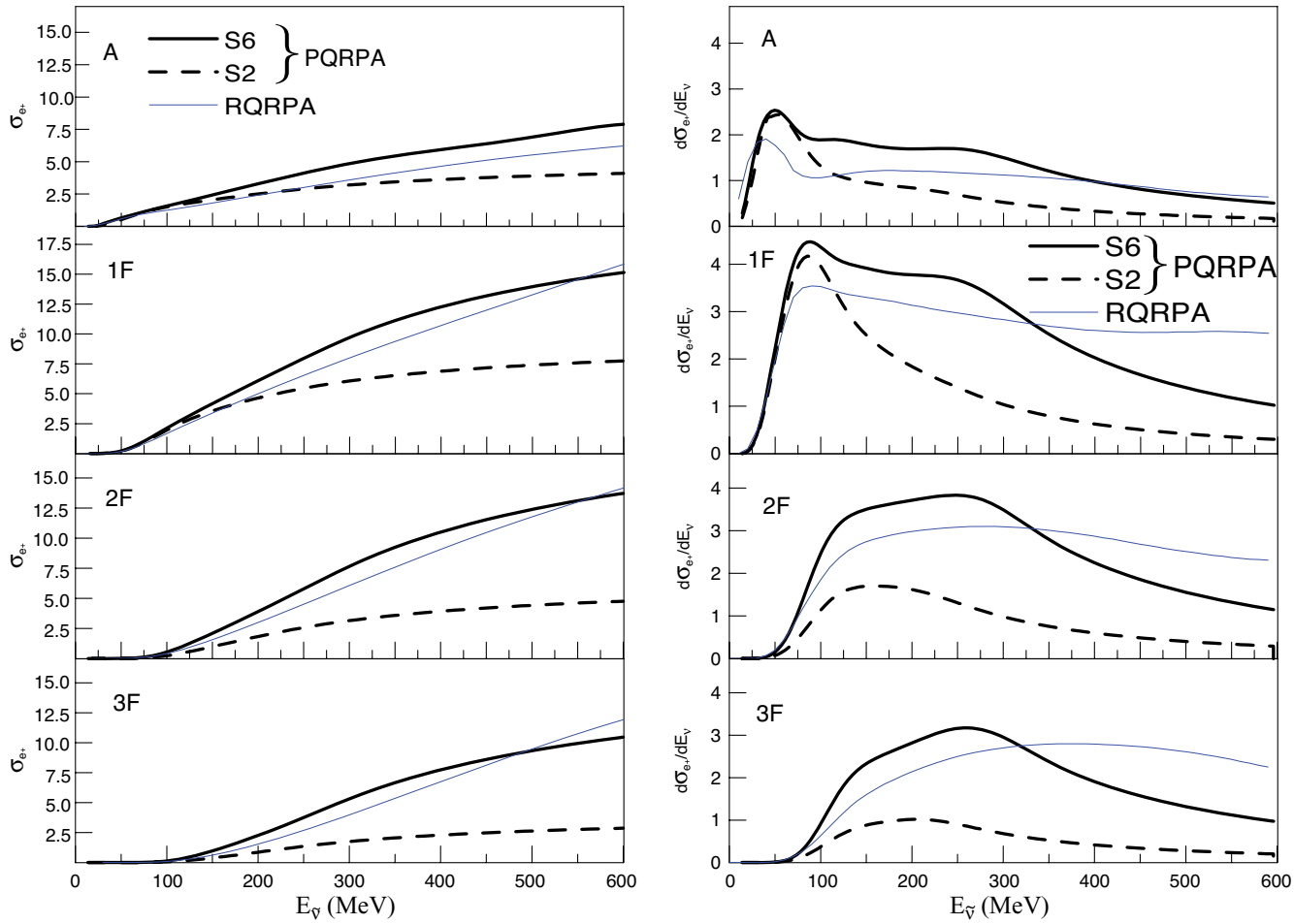

FIG. 12. (Color online) Left: Allowed ($J^\pi = 0^+, 1^+$), first-forbidden ($J^\pi = 0^-, 1^-, 2^-$), second-forbidden ($J^\pi = 2^+, 3^+$), and third-forbidden ($J^\pi = 3^-, 4^-$) inclusive ^{12}C($\tilde{\nu}, e^+$)^{12}B cross section $\sigma_{e^+}(E_{\tilde{\nu}})$ (in units of 10^{-42} cm^2), plotted as a function of the incident neutrino energy $E_{\tilde{\nu}}$. Right: Same as left, but for $d\sigma_{e^+}(E_{\tilde{\nu}})/dE_{\tilde{\nu}}$ (in units of 10^{-42} cm^2 MeV^{-1}).

quite significant even at $E_{\tilde{\nu}} = 500$ MeV.[5] In the case of RQRPA, the spectral function $d\sigma^A_{e^+}(E_{\tilde{\nu}})/dE_{\tilde{\nu}}$ also displays a low-energy resonant structure, and $\sigma^A_{e^+}(E_{\tilde{\nu}})$ is always smaller in magnitude than in the PQRPA case. Third, $\sigma^{1F}_{e^+}(E_{\tilde{\nu}})$ peaks at $E_{\tilde{\nu}} \sim 75$ MeV, and its contribution is always larger than that of $\sigma^A_{e^+}(E_{\tilde{\nu}})$ for $E_{\tilde{\nu}} \gtrsim 150$ MeV. Fourth, $\sigma^{2F}_{e^+}(E_{\tilde{\nu}})$ and $\sigma^{3F}_{e^+}(E_{\tilde{\nu}})$ mainly contribute in the interval $150 \lesssim E_{\tilde{\nu}} \lesssim 400$ MeV, and their overall contributions are of the same order of magnitude, and comparable to that of $\sigma^{1F}_{e^+}(E_{\tilde{\nu}})$. Fifth, the contributions of the remaining multipoles with $J^\pi = 4^+, 5^\pm, 6^\pm, 7^\pm$ are always very small for space S_2 but are quite sizable for S_6 at high energies. For instance, at $E_{\tilde{\nu}} = 100$, 300, and 600 MeV they contribute 0.02%, 0.86%, and 1.18% within space S_2 and 0.04%, 14%, and 20% in S_6. With a further increase in the s.p. basis, configurations from higher multipoles become more pronounced at higher neutrino energies. In particular, the sum of contributions coming from $J^\pi = 4^+, \ldots, 11^\pm$ multipoles, when evaluated within the RQRPA using space S_{30} and a maximal value of $E_{2qp} = 500$ MeV are 1.1%, 14.4%, and 33.2% at $E_\nu = 100$, 300, and 600 MeV, respectively.

Recently Lazauskas and Volpe [108,109] have suggested the convenience of performing nuclear structure studies using low-energy neutrino and antineutrino beams. For feasibility reasons the flux covers only 80 MeV. Nevertheless, from the analysis of ^{16}O, ^{56}Fe, ^{100}Mo, and ^{208}Pb nuclei within the QRPA using the Skyrme force, they were able to disentangle the multipole distributions of forbidden cross sections, showing that the forbidden multipole contribution is different for different nuclei. In this work we extend this kind of study to ^{12}C.

Table I reports results for flux-averaged cross sections $\overline{\sigma}_{e^+}$ for the reaction ^{12}C($\tilde{\nu}, e^+$)^{12}B. In Eq. (2.29) we have used the same antineutrino fluxes $n_{e^+}(E_{\tilde{\nu}})$ as in Ref. [108], that is, the DAR flux, and those produced by boosted ^{6}He ions with different values of time dilation factor $\gamma = 1/\sqrt{1 - v^2/c^2}$. Results of two calculations are presented: the PQRPA within S_6 and (ii) the RQRPA within $N = 20$, with cutoff $E_{2qp} = 300$ MeV. One sees that in both models, principally in

[5]The denominations here do not have exactly the same meaning as in low-energy β decay, where allowed transitions are those within the same HO shell ($\Delta N = 0$), while here all values of ΔN are permitted. The situation is similar for forbidden transitions. The degrees of hindrance basically comes from the value of the orbital angular momenta.

TABLE I. Fraction (in %) of flux-averaged cross sections $\overline{\sigma}_{e^+}$ for ^{12}C($\tilde{\nu}$, e^+)^{12}B for allowed (A), first forbidden (1F), second forbidden (2F), and third forbidden (3F) processes. Antineutrino fluxes $n_{e^+}(E_{\tilde{\nu}})$ are the same as in Ref. [108], that is, the DAR flux, and those produced by boosted ^{6}He ions with different values of $\gamma = 1/\sqrt{1 - v^2/c^2}$. Results of two calculations are presented: (i) PQRPA within S_5 and (ii) RQRPA within $N = 30$, with a cutoff $E_{2qp} = 300$ MeV.

	DAR	γ		
		6	10	14
A				
PQRPA	79.43	92.09	77.00	63.01
RQRPA	84.40	94.88	82.25	67.15
1F				
PQRPA	20.03	7.83	22.16	33.76
RQRPA	15.10	4.13	16.86	29.61
2F				
PQRPA	0.51	0.07	0.78	2.89
RQRPA	0.55	0.08	0.81	2.91
3F				
PQRPA	0.018	0.002	0.04	0.33
RQRPA	0.025	0.011	0.05	0.33

the PQRPA, the allowed transitions dominate the forbidden one, especially for a low-energy beam with $\gamma = 6$. The contributions of the second-forbidden processes are very small in all the cases, while those coming from third-forbidden ones are always negligible. All this is totally consistent with the results shown in Fig. 12, from which it is clear that, to study second and third forbidden reactions in ^{12}C, one would need fluxes $n_{e^+}(E_{\tilde{\nu}})$ with $E_{\tilde{\nu}}$ least up to at $\gtrsim$150 MeV. It should also be stressed that our results for both allowed and forbidden transitions fully agree with those obtained in Ref. [108]; the difference in ^{16}O comes from the double-shell closure in this nucleus.

E. Supernova neutrinos

We also address briefly the $\nu/\tilde{\nu}$-^{12}C nucleus cross sections related to astrophysical applications, the knowledge of which could have important implications. For this purpose, we evaluate the $\overline{\sigma}_{e^\pm}$ folded with supernova $\nu/\tilde{\nu}$ spectra represented by a normalized Fermi-Dirac distribution with temperatures in the interval $T_{\nu_e} = 2$–12 MeV, which includes the most commonly used values, $T_{\nu_e} = 3.2$ MeV and $T_{\tilde{\nu}_e} = 5.0$ MeV. For mean energies $\langle E_\nu \rangle \approx 3.15 \times T_\nu$ and zero chemical potential [110,111], the neutrino flux is

$$n_e(E_\nu) = \frac{0.5546}{T_\nu^3} \frac{E_\nu^2}{e^{E_\nu/T_\nu} + 1}, \tag{3.5}$$

and similarly for antineutrinos. For the sake of simplicity we do not analyze the same relevant aspects of $n_e(E_\nu)$ in supernova simulation, such as the MSW effect (see, e.g., Ref. [112]) and the spectral swapping of the neutrino flux [113]. In Fig. 13 we compare the ν-^{12}C cross sections averaged over supernova ν fluxes for the range of $T_\nu = 2$–12 MeV, obtained in the following calculations:

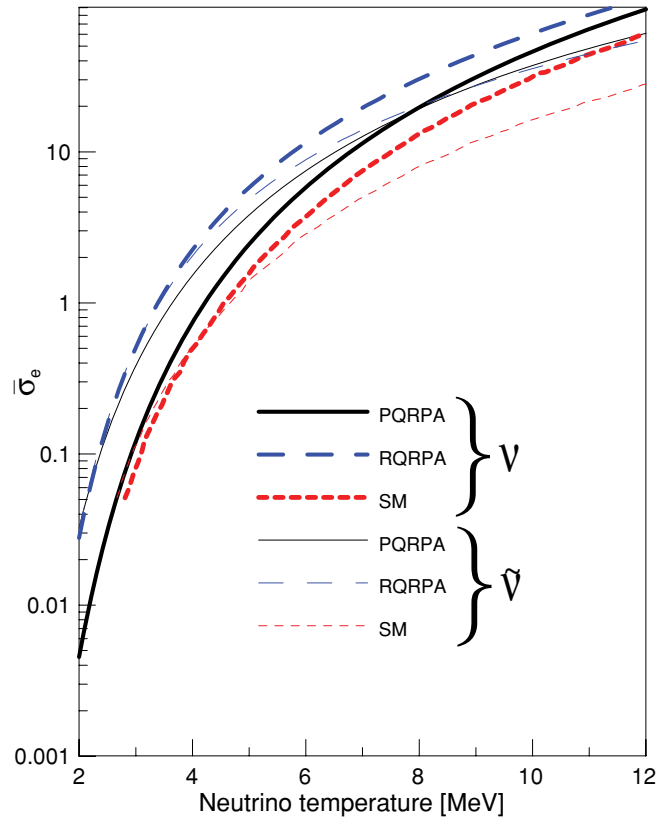

FIG. 13. (Color online) Flux-averaged neutrino and antineutrino cross sections $\overline{\sigma}_{e^\pm}$ in ^{12}C with typical supernova fluxes.

(i) the PQRPA within S_6,
(ii) the RQRPA within S_{30} and $E_{2qp} = 500$ MeV, and
(iii) the SM as used by Suzuki *et al.* [44] with the SFO Hamiltonian (the PSDMK2 interaction yields a quite similar result).

As shown in Fig. 13, in the vicinity of the temperatures mentioned at the beginning ($T_\nu = 3$–5 MeV), these three calculations yield, respectively, that (i) $\overline{\sigma}_{e^+}$ is significantly larger than $\overline{\sigma}_{e^-}$, (ii) $\overline{\sigma}_{e^-}$ is only slightly larger than $\overline{\sigma}_{e^+}$, and (iii) $\overline{\sigma}_{e^+} \cong \overline{\sigma}_{e^-}$. Both SM cross sections are always smaller than those obtained in the the other two calculations, e specially in comparison with the RQRPA one.

IV. SUMMARY AND CONCLUDING REMARKS

The present work is a continuation of our previous work [48,49]. In fact, the formalism for weak interaction processes introduced there is now elaborated more thoroughly, yielding very simple expressions for the transition rates, which greatly facilitate the numerical calculation. This is done through separation of the nuclear matrix elements into their real and imaginary parts, which, in turn, permits splitting of the transition rates for neutrino-nucleus reactions [Eq. (2.22)], into natural [Eq. (A6)] and unnatural parity [Eq. (A7)] operators. A similar separation is done for the muon-capture transition rate [Eq. (D3)] in Eqs. (D4) and (D5). Moreover, consequences of explicit violation of the CVC hypothesis by the Coulomb field

[Eq. (2.18)] are addressed for the first time, and the sum-rule approach for the ICS, proper to the present formalism, is worked out in Appendix B. For the sake of completeness, the extreme relativistic limit of the neutrino-nucleus cross section is also presented in Appendix C, where the formulas for transition rates turn out to be still simpler. We note that, except at very low neutrino energies, they can be used without any restriction in practical applications.

We have discussed in detail the inclusive properties that comprise the following.

(i) Ground-state energies in ^{12}B and ^{12}N and the corresponding GT B values (Fig. 1).
(ii) Exclusive ^{12}C$(\nu, e^-)^{12}$N cross section $\sigma_e(E_\nu, 1^+_1)$, as a function of the incident neutrino energy E_ν (Figs. 2 and 3).
(iii) Exclusive ^{12}C$(\tilde{\nu}, e^+)^{12}$B cross section $\sigma_{e^+}(E_{\tilde{\nu}}, 1^+_1)$, as a function of the incident antineutrino energy $E_{\tilde{\nu}}$ (Fig. 4).
(iv) Muon-capture transition rate to the ^{12}B ground state and electron and muon folded cross sections to the ^{12}N ground states $\overline{\sigma}_\epsilon(1^+_1)$ and $\overline{\sigma}_\mu(1^+_1)$ (Fig. 5).

Special attention was paid to the interplay between the size of the configuration space and the magnitude of the residual interaction within the pp channel. It was found that as the first becomes larger, the second has to increase to obtain agreement with the experimental data for exclusive observables.

The main purpose of our discussion of exclusive properties was to report the limitations of the RPA and the QRPA models. The basic problem in the implementation of the RPA is the lack of pairing correlations, that is, the inability to open the $1p_{3/2}$ shell, while the deficiency of the standard QRPA is in the nonconservation of the number of particles, as evidenced by the wave functions (3.1), (3.2), and (3.3) presented in Sec. III. In this way we have definitively established that the SM and the PQRPA are proper theoretical frameworks in which to describe the ground-state properties of ^{12}B and ^{12}N.[6]

The ICSs ^{12}C$(\nu, e^-)^{12}$N and ^{12}C$(\tilde{\nu}, e^+)^{12}$B have been studied within the PQRPA in the same manner as the exclusive ones for E_{ν_e} up to 300 MeV. As there are no experimental results available in this case the comparison is done with the previous calculations only,[7] and results are displayed in Figs. 6 and 7. Here, unlike in Figs. 2–4, we also show results obtained with the other RPA-like models [34,43,51,102], which could be a suitable framework for description of global nuclear properties as are ICSs.

When the size of the configuration space is enlarged, the calculated PQRPA cross sections, differently from the exclusive ones, steadily increase, particulary for neutrino energies higher than 200 MeV, despite the inclusion of the particle-particle interaction. At low energy they approach the cross section of the first forbidden sum-rule limit but are significantly smaller at high energies for both neutrinos and antineutrinos.

The largest space that we can deal with in the number projection procedure is the one that includes all the orbitals until the $N = 6$ HO shell. This is the reason why we have returned to the RQRPA, wherein it is possible to employ larger configuration spaces. It seems that when the number of shells is increased to $N = 30$, and the cutoff energy E_{2qp} is high enough, the cross sections very likely converge as shown in Figs. 8–11.

Figure 10 also indicates that the RQRPA is a promising nuclear model to reproduce the QE $(\nu_\mu, ^{12}$C) cross section in the region $E_{\nu_\mu} \sim 1$ GeV, which has been measured recently at MiniBooNE [13]. We do not know whether the discrepancy between experiment and theory comes from the noncompleteness of the configuration space or from the smallness of the effective axial-vector coupling constant that we are using, $g_A = 1$. It could also be that we need $g_A = 1$ for the low-energy ECS and $g_A = 1.255$ for the high-energy ICS. We do not understand the reason for this energy dependence of g_A, but it is consistent with Eq. (23) in Ref. [114], where it is shown that for low-energy β decay, g_A could be much more quenched than the total GT strength. We hope to be able to say more on this matter in the near-future.

We have also addressed the issue of the multipole composition of ICSs, by separating them into allowed ($J^\pi = 0^+, 1^+$), first forbidden ($J^\pi = 0^-, 1^-, 2^-$), second forbidden ($J^\pi = 2^+, 3^+$), and third forbidden ($J^\pi = 3^-, 4^-$) processes. The results for the antineutrino reaction ^{12}C$(\tilde{\nu}, e^+)^{12}$B are displayed in Fig. 12 for both the PQRPA and the RQRPA. Of course, similar results are also obtained for neutrinos. We remark that the spectral functions $d\sigma^A_{e^+}(E_{\tilde{\nu}})/dE_{\tilde{\nu}}$, when evaluated within the PQRPA, clearly demonstrate the resonant structure of the allowed cross section, which is mainly of the GT type.

The study of partial ICSs has been related to the proposal made in Refs. [108] and [109] of performing nuclear structure studies of forbidden processes using low-energy neutrino and antineutrino beams. From the results reported in Table I for the flux-averaged cross sections $\overline{\sigma}_{e^+}$ in the reaction ^{12}C$(\tilde{\nu}, e^+)^{12}$B, we show that the contribution of allowed transitions decreases gradually in favor of first forbidden transitions according with the increase in γ boost. We conclude that to study high forbidden reactions, one would need $\tilde{\nu}$ fluxes with $E_{\tilde{\nu}}$ up to $\gtrsim$150 MeV in ^{12}C.

At the end we considered possible astrophysical applications of the $\nu/\tilde{\nu}$-^{12}C nucleus folded cross sections $\overline{\sigma}_{e^\pm}$, using supernova $\nu/\tilde{\nu}$ spectra represented by a normalized Fermi-Dirac distribution with mean energy $\langle E_\nu \rangle \approx 3.15 \times T_\nu$ and zero chemical potential. It is found that for temperature $T_\nu = 3$–5 MeV, both the PQRPA and the RQRPA models yield significantly larger cross sections than the previously used SM.

ACKNOWLEDGMENTS

This work was partially supported by the Argentinean agency CONICET under Contract No. PIP 0377, US DOE

[6] After our work was finished, Cheoun *et al.* [115] presented a new evaluation of the ECS in ^{12}C within the QRPA. They get a good agreement with data for $\overline{\sigma}_e(^{12}$N), which is at variance with the previous QRPA calculation [43].

[7] As mentioned in Sec. I, the only available experimental data on the ^{12}C electron-neutrino ICS is the low-energy ($E_{\nu_e} < 60$ MeV) folded one, which has been discussed in our previous work [49–51].

Grant Nos. DE-FG02-08ER41533 and DE-FC02-07ER41457 (UNEDF, SciDAC-2), and the Research Corporation. A.R.S. thanks W. C. Haxton and G. M. Fuller for stimulating discussion and the Institute of Nuclear Theory of University of Washington, where part of this work was performed. N.P. acknowledges support from the Unity through Knowledge Fund (UKF Grant No. 17/08), MZOS Project No. 1191005-1010, and the Croatian National Foundation for Science.

APPENDIX A: CONTRIBUTIONS TO $\mathcal{T}_{J^\pi_n}(\kappa)$ OF NATURAL AND UNNATURAL PARITY STATES

The real and imaginary parts of the operators $\mathsf{O}_{\alpha\mathsf{J}}$ given by Eqs. (2.12) and (2.20) do not contribute simultaneously. In fact, $\Re\mathsf{O}_{\alpha\mathsf{J}}$ ($\Im\mathsf{O}_{\alpha\mathsf{J}}$) contributes to natural (unnatural) parity states, which means that we can always work only with real operators, which greatly simplifies the calculations. To see this we note that, while the operators $\mathcal{M}^V_{\mathsf{J}}$, $\mathcal{M}^A_{\mathsf{J}}$, and

$$\mathcal{M}^A_{0\mathsf{J}} = \sum_{\mathsf{L}=\mathsf{J}\pm1} (-)^{(\mathsf{J}-\mathsf{L}-1)/2}\, F_{\mathsf{L}\mathsf{J}0}\, j_{\mathsf{L}}(\rho)[Y_{\mathsf{L}}(\hat{\mathbf{r}})\otimes\boldsymbol{\sigma}]_{\mathsf{J}} \tag{A1}$$

are real, $\mathcal{M}^A_{\pm1\mathsf{J}}$ and $\mathcal{M}^V_{\pm1\mathsf{J}}$ are not. Explicitly,

$$\begin{aligned}\mathcal{M}^A_{\pm1\mathsf{J}} &= \mathcal{M}^{A,R}_{\pm1\mathsf{J}} + i\mathcal{M}^{A,I}_{\pm1\mathsf{J}},\\ \mathcal{M}^V_{\pm1\mathsf{J}} &= \mathcal{M}^{V,R}_{\pm1\mathsf{J}} + i\mathcal{M}^{V,I}_{\pm1\mathsf{J}},\end{aligned} \tag{A2}$$

where

$$\begin{aligned}\mathcal{M}^{A,R}_{1\mathsf{J}} &\equiv \mathcal{M}^{A,R}_{-1\mathsf{J}}\\ &= \sum_{\mathsf{L}=\mathsf{J}\pm1} (-)^{(\mathsf{J}-\mathsf{L}-1)/2}\, F_{\mathsf{L}\mathsf{J}1}\, j_{\mathsf{L}}(\rho)[Y_{\mathsf{L}}(\hat{\mathbf{r}})\otimes\boldsymbol{\sigma}]_{\mathsf{J}},\\ \mathcal{M}^{A,I}_{1\mathsf{J}} &\equiv -\mathcal{M}^{A,I}_{-1\mathsf{J}} = -F_{1\mathsf{J}\mathsf{J}}\, j_{\mathsf{J}}(\rho)[Y_{\mathsf{J}}(\hat{\mathbf{r}})\otimes\boldsymbol{\sigma}]_{\mathsf{J}},\\ \mathcal{M}^{V,R}_{1\mathsf{J}} &\equiv \mathcal{M}^{V,R}_{-1\mathsf{J}}\\ &= \sum_{\mathsf{L}=\mathsf{J}\pm1} (-)^{(\mathsf{J}-\mathsf{L}-1)/2}\, F_{\mathsf{L}\mathsf{J}1}\, j_{\mathsf{L}}(\rho)[Y_{\mathsf{L}}(\hat{\mathbf{r}})\otimes\boldsymbol{\nabla}]_{\mathsf{J}},\\ \mathcal{M}^{V,I}_{1\mathsf{J}} &\equiv -\mathcal{M}^{V,I}_{-1\mathsf{J}} = -F_{1\mathsf{J}\mathsf{J}}\, j_{\mathsf{J}}(\rho)[Y_{\mathsf{J}}(\hat{\mathbf{r}})\otimes\boldsymbol{\nabla}]_{\mathsf{J}},\end{aligned} \tag{A3}$$

with $\mathsf{L}\geqslant 0$, and $\mathsf{J}\neq 0$. Thus

$$\begin{aligned}\mathsf{O}_{\pm1\mathsf{J}} = i(-g_{\mathrm{A}} \pm \overline{g}_{\mathrm{W}})\big(\mathcal{M}^{A,R}_{1\mathsf{J}} \pm i\mathcal{M}^{A,I}_{1\mathsf{J}}\big)\\ + g_V\big(\mathcal{M}^{V,R}_{1\mathsf{J}} \pm i\mathcal{M}^{V,I}_{1\mathsf{J}}\big),\end{aligned} \tag{A4}$$

and writing

$$\begin{aligned}\mathsf{O}_{\emptyset\mathsf{J}} &= \mathsf{O}^R_{\emptyset\mathsf{J}} + i\mathsf{O}^I_{\emptyset\mathsf{J}},\\ \mathsf{O}_{m\mathsf{J}} &= \mathsf{O}^R_{m\mathsf{J}} + i\mathsf{O}^I_{m\mathsf{J}},\end{aligned} \tag{A5}$$

it is not difficult to discover the following.

(i) *For natural parity states*, with $\pi = (-)^J$, that is, $J^\pi = 0^+, 1^-, 2^+, 3^-, \ldots$:

$$\begin{aligned}\mathsf{O}^R_{\emptyset\mathsf{J}} &= g_V\mathcal{M}^V_{\mathsf{J}},\\ \mathsf{O}^R_{0\mathsf{J}} &= \frac{\tilde{k}_\emptyset}{\kappa} g_{\mathrm{V}}\mathcal{M}^V_{\mathsf{J}},\\ \mathsf{O}^R_{\pm1\mathsf{J}} &= (\pm g_{\mathrm{A}} - \overline{g}_{\mathrm{W}})\mathcal{M}^{A,I}_{1\mathsf{J}} + g_V\mathcal{M}^{V,R}_{1\mathsf{J}}.\end{aligned} \tag{A6}$$

(ii) *For unnatural parity states*, with $\pi = (-)^{J+1}$, that is, $J^\pi = 0^-, 1^+, 2^-, 3^+, \ldots$:

$$\begin{aligned}\mathsf{O}^I_{\emptyset\mathsf{J}} &= -g_A\mathcal{M}^A_{\mathsf{J}} - (\overline{g}_{\mathrm{A}} + \overline{g}_{\mathrm{P1}})\mathcal{M}^A_{0\mathsf{J}},\\ \mathsf{O}^I_{0\mathsf{J}} &= (g_{\mathrm{A}} - \overline{g}_{\mathrm{P2}})\mathcal{M}^A_{0\mathsf{J}},\\ \mathsf{O}^I_{\pm1\mathsf{J}} &= (g_{\mathrm{A}} \mp \overline{g}_{\mathrm{W}})\mathcal{M}^{A,R}_{1\mathsf{J}} \mp g_{\mathrm{V}}\mathcal{M}^{V,I}_{1\mathsf{J}}.\end{aligned} \tag{A7}$$

These operators have to be used in Eq. (2.22), instead of those defined in Eqs. (2.12) and (2.20).

The correspondence between the individual matrix elements, defined by Donnelly, and Peccei in Eq (3.31) of Ref. [77], and the ones used here is

$$\begin{aligned}&M_{\mathsf{J}} \to \mathcal{M}^V_{\mathsf{J}}, \quad \Delta_{\mathsf{J}} \to \sqrt{2}\mathcal{M}^{V,I}_{1\mathsf{J}}, \quad \Delta'_{\mathsf{J}} \to -\sqrt{2}\mathcal{M}^{V,R}_{1\mathsf{J}},\\ &\Sigma_{\mathsf{J}} \to \sqrt{2}\mathcal{M}^{A,I}_{1\mathsf{J}}, \quad \Sigma'_{\mathsf{J}} \to -\sqrt{2}\mathcal{M}^{A,R}_{1\mathsf{J}},\\ &\Sigma''_{\mathsf{J}} \to \mathcal{M}^A_{0\mathsf{J}}, \quad \Omega_{\mathsf{J}} \to \mathcal{M}^A_{\mathsf{J}}.\end{aligned} \tag{A8}$$

Moreover, the correspondence between the linear combinations of these matrix elements defined in Eqs. (3.32) of Ref. [77] (for $\hat{L}_{\mathsf{J}}$ see Eq. (14) of Ref. [79]) and the ones introduced here is as follows.

(i) *For natural parity states*,

$$\begin{aligned}\hat{M}_{\mathsf{J}} = \mathsf{O}_{\emptyset\mathsf{J}}, \quad \hat{L}_{\mathsf{J}} = \mathsf{O}_{0\mathsf{J}},\\ \hat{T}^{\mathrm{el}}_{\mathsf{J}} \pm \hat{T}^{\mathrm{mag5}}_{\mathsf{J}} = -\sqrt{2}\mathsf{O}_{\pm1\mathsf{J}}.\end{aligned} \tag{A9}$$

(ii) *For unnatural parity states*,

$$\begin{aligned}\hat{M}^5_{\mathsf{J}} = \mathsf{O}_{\emptyset\mathsf{J}}, \quad -i\hat{L}^5_{\mathsf{J}} = \mathsf{O}_{0\mathsf{J}},\\ i(\hat{T}^{\mathrm{el5}}_{\mathsf{J}} \pm \hat{T}^{\mathrm{mag}}_{\mathsf{J}}) = \sqrt{2}\mathsf{O}_{\pm1\mathsf{J}}.\end{aligned} \tag{A10}$$

The following relation can also be useful:

$$\begin{aligned}\mathsf{O}_{\emptyset\mathsf{J}} &= \hat{\mathcal{M}}_{\mathsf{J}},\\ \mathsf{O}_{m\mathsf{J}} &= \begin{cases}\hat{\mathcal{L}}_{\mathsf{J}}, & \text{for} \quad m=0,\\ -\frac{1}{\sqrt{2}}\big[m\hat{T}^{\mathrm{mag}}_{\mathsf{J}} + \hat{T}^{\mathrm{el}}_{\mathsf{J}}\big] & \text{for} \quad m=\pm1,\end{cases}\end{aligned} \tag{A11}$$

where $\hat{\mathcal{M}}_{\mathsf{J}} = \hat{M}_{\mathsf{J}} + \hat{M}^5_{\mathsf{J}}$, $\hat{\mathcal{L}}_{\mathsf{J}} = \hat{L}_{\mathsf{J}} + \hat{L}^5_{\mathsf{J}}$, $\hat{T}^{\mathrm{el}}_{\mathsf{J}} = \hat{T}^{\mathrm{el}}_{\mathsf{J}} + \hat{T}^{\mathrm{el5}}_{\mathsf{J}}$, and $\hat{T}^{\mathrm{mag}}_{\mathsf{J}} = \hat{T}^{\mathrm{mag}}_{\mathsf{J}} + \hat{T}^{\mathrm{mag5}}_{\mathsf{J}}$.

The matrix elements of Kuramoto *et al.* [74] are related to our nonrelativistic operators, Eq. (2.14), as

$$\begin{aligned}|\langle f|\hat{1}|i\rangle|^2 &= 4\pi\sum_{\mathsf{J}^\pi_n}\big|\big\langle \mathsf{J}^\pi_n\big|\big|\mathcal{M}^V_{\mathsf{J}}\big|\big|0^+\big\rangle\big|^2,\\ |\langle f|\hat{\sigma}|i\rangle|^2 &= 4\pi\sum_{\mathsf{J}^\pi_n}\sum_{m=0,\pm1}\big|\big\langle \mathsf{J}^\pi_n\big|\big|\mathcal{M}^A_{m\mathsf{J}}\big|\big|0^+\big\rangle\big|^2,\\ \Lambda &= \frac{4\pi}{3}\sum_{\mathsf{J}^\pi_n}\Big[\big|\big\langle \mathsf{J}^\pi_n\big|\big|\mathcal{M}^A_{0\mathsf{J}}\big|\big|0^+\big\rangle\big|^2\\ &\quad - \big|\big\langle \mathsf{J}^\pi_n\big|\big|\mathcal{M}^A_{1\mathsf{J}}\big|\big|0^+\big\rangle\big|^2\Big].\end{aligned} \tag{A12}$$

In Ref. [74] the relativistic operators $\mathcal{M}^A_{\mathsf{J}}$, and $\mathcal{M}^V_{m\mathsf{J}}$ defined in Eq. (2.15) are neglected.

APPENDIX B: SUM-RULE APPROACH

We follow here the sum-rule approach developed by Kuramoto *et al.* [74] and adapt it to our formalism. We start

from Eqs. (2.25) and (2.27), and as in this work, we assume that the $\omega_{J_n^\pi}$ dependence of the integrand can be ignored, fixing it at a representative value $\overline{\omega_{J_n^\pi}}$. The summation over final nuclear states J_n^π then can be carried out by closure, and the ICS is

$$\sigma_\ell^{\rm SR}(E_\nu) = G^2 \frac{|\mathbf{p}_\ell| E_\ell}{2\pi} F(Z+S, E_\ell) \int_{-1}^{1} d(\cos\theta) \mathcal{T}^{\rm SR}, \tag{B1}$$

where the lepton energy is $E_\ell = E_\nu - \overline{\omega_{J_n^\pi}}$, while the sum-rule matrix element reads

$$\mathcal{T}^{\rm SR} = \sum_{\alpha=\emptyset,0,\pm1} \langle 0^+|O_\alpha^\dagger O_\alpha|0^+\rangle \mathcal{L}_\alpha - 2\Re(\langle 0^+|O_\emptyset^\dagger O_0|0^+\rangle \mathcal{L}_{\emptyset 0}). \tag{B2}$$

The operators O_α are given by Eq. (2.6), and the lepton traces by Eq. (2.24) of Ref. [49]. The matrix elements in Eq. (B2) are proportional to $N(1-D)$, where N_N is the number of neutrons (protons), contained in the target nucleus for the neutrino (antineutrino) reaction. The correlation functions D come from the Pauli exclusion effect and depend on the type of the operator. One gets

$$\mathcal{T}^{\rm SR} = N_N \left(T_\emptyset \mathcal{L}_\emptyset + \sum_M T_M \mathcal{L}_M - 2T_{\emptyset 0}\mathcal{L}_{\emptyset 0} \right), \tag{B3}$$

with

$$\begin{aligned} T_\emptyset &\equiv g_{\rm V}^2(1-D_S) + (\overline{g}_{\rm A} + \overline{g}_{\rm P1})^2(1-D_L), \\ T_0 &\equiv \overline{g}_{\rm V}^2(1-D_S) + (g_{\rm A} - \overline{g}_{\rm P2})^2(1-D_L), \\ T_1 &\equiv (g_{\rm A} - \overline{g}_{\rm W})^2(1-D_T), \\ T_{-1} &\equiv (g_{\rm A} + \overline{g}_{\rm W})^2(1-D_T), \\ T_{\emptyset 0} &\equiv -g_{\rm V}\overline{g}_{\rm V}(1-D_S) + (\overline{g}_{\rm A} + \overline{g}_{\rm P1})(g_{\rm A} - \overline{g}_{\rm P2})(1-D_L). \end{aligned} \tag{B4}$$

The correlation functions D_S, D_L, and D_S were taken from the SM calculation done by Bell and Llewellyn Smith [116] with HO wave functions and representing the nuclear ground state by a single determinant wave function. The results for ^{12}C are (see Table I in Ref. [116]:

$$\begin{aligned} D_S &= e^{-\eta}[1 + 0.148\eta^2], \\ D_T &= e^{-\eta}[0.704 + 0.148\eta + 0.148\eta^2], \\ D_L &= e^{-\eta}[0.704 + 0.296\eta + 0.148\eta^2], \end{aligned} \tag{B5}$$

where $\eta = \frac{1}{2}b^2\kappa^2 \cong 0.0558$.

As seen from Eq. (2.26), the factor $|\mathbf{p}_\ell|E_\ell$ in Eq. (B1) behaves as $(E_\nu - \overline{\omega_{J_n^\pi}})^2$, and therefore $\sigma_\ell^{\rm SR}(E_\nu)$ depends very critically on the average value for the excitation energy $\overline{\omega_{J_n^\pi}}$.

$$\begin{aligned} E_\ell &= E_\nu - \omega_{J_n^\pi}, |\mathbf{p}_\ell| = \sqrt{\left(E_\nu - \omega_{J_n^\pi}\right)^2 - m_\ell^2}, \\ \kappa &= |\mathbf{p}_\ell - \mathbf{q}_\nu| \\ &= \sqrt{2E_\nu(E_\ell - |\mathbf{p}_\ell|\cos\theta) - m_\ell^2 + \omega_{J_n^\pi}^2}, \end{aligned} \tag{B6}$$

APPENDIX C: EXTREME RELATIVISTIC LIMIT

Using the present formalism the ERL, defined by the limit of the lepton velocity $|\mathbf{p}_\ell|/E_\ell \to 1$, yields

$$\sigma_\ell^{\rm ERL}(E_\nu) = \sum_{J_n^\pi} \frac{E_\ell^2}{2\pi} F(Z+S, E_\ell) \int_{-1}^{1} d(\cos\theta) \mathcal{T}_{J_n^\pi}^{\rm ERL}(\kappa), \tag{C1}$$

with

$$\kappa = \sqrt{2E_\nu E_\ell(1-\cos\theta) + \omega_{J_n^\pi}^2}, \tag{C2}$$

and

$$\begin{aligned} \mathcal{T}_{J_n^\pi}^{\rm ERL}(\kappa) = 4\pi G^2 \Bigg[& 2\cos^2\frac{\theta}{2} \left| \langle J_n^\pi || \mathsf{O}_{\emptyset \mathsf{J}}(\kappa) - \frac{k_\emptyset}{\kappa} \mathsf{O}_{0\mathsf{J}}(\kappa) || 0^+ \rangle \right|^2 \\ & + \sum_{m=\pm1} \left| \langle J_n^\pi || \mathsf{O}_{m\mathsf{J}}(\kappa) || 0^+ \rangle \right|^2 \left(\frac{k^2}{\kappa^2}\cos^2\frac{\theta}{2} \right. \\ & \left. + 2\sin^2\frac{\theta}{2} + 2mS\sin\frac{\theta}{2}\sqrt{\frac{k^2}{\kappa^2}\cos^2\frac{\theta}{2} + \sin^2\frac{\theta}{2}} \right) \Bigg]. \end{aligned} \tag{C3}$$

APPENDIX D: MUON-CAPTURE RATE

For the sake of completeness we also show the formula for the muon-capture process within the present formalism. Here $\kappa = E_\nu = \mathrm{m}_\mu - \omega_{J_n^\pi} - \Delta\mathrm{M} - E_B$, where E_B^μ is the binding energy of the muon in the $1S$ orbit, and instead of Eq. (2.5), one has

$$\begin{aligned} \overline{g}_{\rm V} &= g_{\rm V}\frac{E_\nu}{2\mathrm{M}}, \quad \overline{g}_{\rm A} = g_{\rm A}\frac{E_\nu}{2\mathrm{M}}, \\ \overline{g}_{\rm W} &= (g_{\rm V} + g_{\rm M})\frac{E_\nu}{2\mathrm{M}}, \quad \overline{g}_{\rm P} = g_{\rm P}\frac{E_\nu}{2\mathrm{M}}, \end{aligned} \tag{D1}$$

where $\overline{g}_{\rm P} = \overline{g}_{\rm P2} - \overline{g}_{\rm P1}$. The muon-capture transition rate reads

$$\Lambda(\omega_{J_n^\pi}) = \frac{E_\nu^2}{2\pi}|\phi_{1S}|^2 \mathcal{T}_\Lambda\left(\omega_{J_n^\pi}\right), \tag{D2}$$

where ϕ_{1S} is the muonic bound-state wave function evaluated at the origin, and

$$\begin{aligned} \mathcal{T}_\Lambda\left(\omega_{J_n^\pi}\right) = 4\pi G^2 \Big[& \left| \langle J_n^\pi || \mathsf{O}_{\emptyset \mathsf{J}}(E_\nu) - \mathsf{O}_{0\mathsf{J}}(E_\nu) || 0^+ \rangle \right|^2 \\ & + 2\left| \langle J_n^\pi || \mathsf{O}_{-1\mathsf{J}}(E_\nu) || 0^+ \rangle \right|^2 \Big], \end{aligned} \tag{D3}$$

with:

(i) *For natural parity states*, with $\pi = (-)^J$, that is, $J^\pi = 0^+, 1^-, 2^+, 3^-, \ldots$:

$$\begin{aligned} \mathsf{O}_{\emptyset \mathsf{J}} - \mathsf{O}_{0,\mathsf{J}} &= g_{\rm V}\frac{\mathrm{m}_\mu - \Delta E_{\rm Coul} - E_B}{E_\nu}\mathcal{M}_{\mathsf{J}}^V, \\ \mathsf{O}_{-1\mathsf{J}} &= -(g_{\rm A} + \overline{g}_{\rm W})\mathcal{M}_{-1\mathsf{J}}^{A,I} + g_{\rm V}\mathcal{M}_{-1\mathsf{J}}^{V,R}. \end{aligned} \tag{D4}$$

(ii) *For unnatural parity states*, with $\pi = (-)^{J+1}$, that is, $J^\pi = 0^-, 1^+, 2^-, 3^+, \ldots$:

$$\begin{aligned} \mathsf{O}_{\emptyset \mathsf{J}} - \mathsf{O}_{0,\mathsf{J}} &= g_{\rm A}\mathcal{M}_{\mathsf{J}}^A + \left(g_{\rm A} + \overline{g}_{\rm A} - \overline{g}_{\rm P}\right)\mathcal{M}_{0\mathsf{J}}^A, \\ \mathsf{O}_{-1\mathsf{J}} &= -(g_{\rm A} + \overline{g}_{\rm W})\mathcal{M}_{-1\mathsf{J}}^{A,R} - g_{\rm V}\mathcal{M}_{-1\mathsf{J}}^{V,I}. \end{aligned} \tag{D5}$$

[1] C. Athanassopoulos *et al.* (LSND Collaboration), Phys. Rev. C **54**, 2685 (1996); Phys. Rev. Lett. **77**, 3082 (1996).
[2] C. Athanassopoulos *et al.* (LSND Collaboration), Phys. Rev. C **58**, 2489 (1998); Phys. Rev. Lett. **81**, 1774 (1998).
[3] A. Aguilar *et al.* (LSND Collaboration), Phys. Rev. D **64**, 112007 (2001).
[4] Y. Fukuda *et al.* (Super-Kamiokande Collaboration), Phys. Rev. Lett. **81**, 1562 (1998); Y. Ashie *et al.* (Super-Kamiokande Collaboration), *ibid.* **93**, 101801 (2004).
[5] B. Aharmim *et al.* (SNO Collaboration), Phys. Rev. C **72**, 055502 (2005); M. B. Smy *et al.* (Super-Kamiokande Collaboration), Phys. Rev. D **69**, 011104 (2004).
[6] T. Araki *et al.* (KamLAND Collaboration), Phys. Rev. Lett. **94**, 081801 (2005).
[7] M. H. Ahn *et al.* (K2K Collaboration), Phys. Rev. Lett. **90**, 041801 (2003).
[8] R. Maschuw *et al.* (KARMEN Collaboration), Prog. Part. Phys. **40**, 183 (1998) , and references therein mentioned.
[9] B. Armbruster *et al.* (KARMEN Collaboration), Phys. Rev. D **65**, 112001 (2002).
[10] R. C. Allen *et al.*, Phys. Rev. Lett. **64**, 1871 (1990).
[11] D. A. Krakauer *et al.*, Phys. Rev. C **45**, 2450 (1992).
[12] A. A. Aguilar-Arevalo *et al.* (SciBooNE Collaboration), arXiv:hep-ex/0601022.
[13] A. A. Aguilar-Arevalo *et al.* (MiniBooNE Collaboration), Nucl. Instrum. Methods A **599**, 28 (2009).
[14] Y. Efremenko, Nucl. Phys. B, Proc. Suppl. **138**, 343 (2005); F. T. Avignone III and Y. V. Efremenko, J. Phys. G **29**, 2615 (2003).
[15] N. Yu Agafonova *et al.*, Astron. Phys. **27**, 254 (2007).
[16] M. Fukugita, Y. Kohyama, and K. Kubodera, Phys. Lett. B **212**, 139 (1988).
[17] D. Autiero *et al.*, J. Cosmol. Astropart. Phys. 11 (2007) 011.
[18] C. Lunardini and A. Y. Smirnov, J. Cosmol. Astropart. Phys. 06 (2003) 009.
[19] A. S. Dighe, M. T. Keil, and G. G. Raffelt, J. Cosmol. Astropart. Phys. 06 (2003) 005.
[20] H. Duan, G. M. Fuller, J. Carlson, and Y.-Z. Qian, Phys. Rev. Lett. **99**, 241802 (2007).
[21] B. Dasgupta, A. Dighe, and A. Mirizzi, Phys. Rev. Lett. **101**, 171801 (2008).
[22] B. Dasgupta, A. Mirizzi, I. Tamborra, and R. Tomas, Phys. Rev. D **81**, 093008 (2010).
[23] M. Mezzetto and T. Schwetz, arXiv:1003.5800v1 [hep-ph].
[24] A. Strumia and F. Vissani, arXiv:hep-ph/0606054v3.
[25] C. Athanassopoulos *et al.* (LSND Collaboration), Phys. Rev. C **55**, 2078 (1997).
[26] L. B. Auerbach *et al.* (LSND Collaboration), Phys. Rev. C **64**, 065501 (2001).
[27] B. Zeitnitz *et al.* (KARMEN Collaboration), Prog. Part. Nucl. Phys. **40**, 169 (1998).
[28] C. Athanassopoulus *et al.* (LSND Collaboration), Phys. Rev. C **56**, 2806 (1997).
[29] L. B. Auerbach *et al.* (LSND Collaboration), Phys. Rev. C **66**, 015501 (2002).
[30] LSND home page [http://www.nu.to.infn.it/exp/all/lsnd/].
[31] Teppei Katori, in *The 5th International Workshop on Neutrino-Nucleus Interactions in the Few-GeV. Region*, edited by Geralyn P. Zeller, Jorge G. Morfin, and Flavio Cavanna, AIP. Conf. Proc. No. 967 (AIP, New York, 2007), p. 123; A. A. Aguilar-Arevalo *et al.*, Phys. Rev. Lett. **103**, 081801 (2009); Phys. Rev. D **81**, 013005 (2010).
[32] A. Rodriguez *et al.* Phys. Rev. D **78**, 032003 (2008).
[33] Y. Kurimoto *et al.*, Phys. Rev. D **81**, 033004 (2010).
[34] J. S. O'Connell, T. W. Donelly, and J. D. Walecka, Phys. Rev. C **6**, 719 (1972).
[35] T. W. Donelly, Phys. Rev. C **1**, 853 (1970).
[36] B. A. Brown and B. H. Wildenthal, At. Data Nucl. Data Tables **33**, 347 (1985).
[37] H. Castillo and F. Krmpotić, Nucl. Phys. A **469**, 637 (1987).
[38] F. Osterfeld, Rev. Mod. Phys. **64**, 491 (1992) , and references therein.
[39] G. Martínez-Pinedo, A. Poves, E. Caurier, and A. P. Zuker, Phys. Rev. C **53**, R2602 (1996).
[40] E. Kolbe, K. Langanke, and S. Krewald, Phys. Rev. C **49**, 1122 (1994).
[41] E. Kolbe, K. Langanke, and P. Vogel, Phys. Rev. C **50**, 2576 (1994).
[42] A. C. Hayes and I. S. Towner, Phys. Rev. C **61**, 044603 (2000).
[43] C. Volpe, N. Auerbach, G. Colò, T. Suzuki, and N. Van Giai, Phys. Rev. C **62**, 015501 (2000).
[44] T. Suzuki, S. Chiba, T. Yoshida, T. Kajino, and T. Otsuka, Phys. Rev. C **74**, 034307 (2006).
[45] G. H. Miller *et al.*, Phys. Lett. B **41**, 50 (1972).
[46] D. F. Measday, Phys. Rep. **354**, 243 (2001).
[47] T. J. Stocki *et al.*, Nucl. Phys. A **697**, 55 (2002).
[48] F. Krmpotić, A. Mariano, and A. Samana, Phys. Lett. B **541**, 298 (2002).
[49] F. Krmpotić, A. Samana, and A. Mariano, Phys. Rev. C **71**, 044319 (2005).
[50] A. Samana, F. Krmpotić, A. Mariano and R. Zukanovich Funchal, Phys. Lett. B **642**, 100 (2006).
[51] N. Paar, D. Vretenar, T. Marketin, and P. Ring, Phys. Rev. C **77**, 024608 (2008).
[52] T. Marketin, N. Paar, T. Nikšić and D. Vretenar, Phys. Rev. C **79**, 054323 (2009).
[53] K. Hagino and H. Sagawa, Nucl. Phys. A **695**, 82 (2001).
[54] V. Rodin and A. Faessler, Phys. Rev. C **77**, 025502 (2008).
[55] R. A. Smith and E. J. Moniz, Nucl. Phys. B **43**, 605 (1972).
[56] J. Nieves, J. E. Amaro, and M. Valverde, Phys. Rev. C **70**, 055503 (2004).
[57] M. Valverde, J. E. Amaro, and J. Nieves, Phys. Lett. B **638**, 325 (2006).
[58] C. Mahaux, P. E. Bortignon, R. A. Broglia, and C. H. Dasso, Phys. Rep. **120**, 1 (1985).
[59] G. Jacob and T. A. J. Maris, Rev. Mod. Phys. **45**, 6 (1973).
[60] S. Frullani and J. Mougey, Adv. Nucl. Phys. **14**, 1 (1984).
[61] S. L. Belostotskii *et al.*, Sov. J. Nucl. Phys. **41**, 903 (1985); S. S. Volkov *et al.*, *ibid.* **49**, 848 (1990).
[62] M. Leuschner *et al.*, Phys. Rev. C **49**, 955 (1994).
[63] T. Yamada, M. Takahashi, and K. Ikeda, Phys. Rev. C **53**, 752 (1996).
[64] T. Yamada, Nucl. Phys. A **687**, 297c (2001).
[65] M. Yosoi *et al.*, Phys. Lett. B **551**, 255 (2003).
[66] T. Yamada, M. Yosoi, and H. Toyokawa, Nucl. Phys. A **738**, 323 (2004).
[67] K. Kobayashi *et al.*, arXiv:nucl-ex/0604006.
[68] J. E. Amaro, M. B. Barbaro, J. A. Caballero, T. W. Donnelly, and C. Maieron, Phys. Rev. C **71**, 065501 (2005).

[69] E. Kolbe, K. Langanke, G. Martínez-Pinedo, and P. Vogel, J. Phys. G **29**, 2569 (2003).
[70] K. S. Kim, M.-K. Cheoun, and B. G. Yu, Phys. Rev. C **77**, 054604 (2008).
[71] A. V. Butkevich, Phys. Rev. C **78**, 015501 (2008); **80**, 014610 (2009); **82**, 055501 (2010).
[72] T. Leitner, O. Buss, and L. Alvarez-Ruso, and U. Mosel, Phys. Rev. C **79**, 034601 (2009).
[73] M. Martini, M. Ericson, G. Chanfray, and J. Marteau, Phys. Rev. C **80**, 065501 (2009).
[74] T. Kuramoto, M. Fukugita, Y. Kohyama, and K. Kubodera, Nucl. Phys. A **512**, 711 (1990).
[75] P. Vogel and M. R. Zirnbauer, Phys. Rev. Lett. **57**, 3148 (1986).
[76] D. Cha, Phys. Rev. C **27**, 2269 (1983).
[77] T. W. Donnelly and R. D. Peccei, Phys. Rep. **50**, 1 (1979).
[78] J. D. Walecka, *Theoretical Nuclear and Subnuclear Physics* (Oxford University Press, New York, 1995), p. 531.
[79] T. W. Donnelly and W. C. Haxton, At. Data Nucl. Data Tables **23**, 103 (1979).
[80] F. Krmpotić, K. Ebert, and W. Wild, Nucl. Phys. A **342**, 497 (1980); F. Krmpotić, Phys. Rev. Lett. **46**, 1261 (1981).
[81] H. Behrens and W. Bühring, *Electron Radial Wave Functions and Nuclear Beta Decay* (Clarendon, Oxford, 1982), and references therein.
[82] R. J. Blin-Stoyle and S. C. K. Nair, Adv. Phys. **15**, 493 (1966).
[83] J. Engel, Phys. Rev. C **57**, 2004 (1998).
[84] A. R. Samana and C. A. Bertulani, Phys. Rev. C **78**, 024312 (2008)
[85] J. Hirsch and F. Krmpotić, Phys. Rev. C **41**, 792 (1990); Phys. Lett. B **246**, 5 (1990).
[86] F. Krmpotić, J. Hirsch, and H. Dias, Nucl. Phys. A **542**, 85 (1992).
[87] F. Krmpotić, A. Mariano, T. T. S. Kuo, and K. Nakayama, Phys. Lett. B **319**, 393 (1993).
[88] F. Krmpotić and S. Sharma, Nucl. Phys. A **572**, 329 (1994).
[89] A. R. Samana, F. Krmpotić, and C. A. Bertulani, Comput. Phys. Commun. **181**, 1123 (2010).
[90] N. Paar, T. Nikšić, D. Vretenar, and P. Ring, Phys. Rev. C **69**, 054303 (2004).
[91] G. A. Lalazissis, T. Nikšić, D. Vretenar, and P. Ring, Phys. Rev. C **71**, 024312 (2005).
[92] J. F. Berger, M. Girod, and D. Gogny, Comput. Phys. Commun. **63**, 365 (1991).
[93] N. Paar, P. Ring, T. Nikšić, and D. Vretenar, Phys. Rev. C **67**, 034312 (2003).
[94] N. Paar, D. Vretenar, E. Khan, and G. Colò, Rep. Prog. Phys. **70**, 691 (2007).
[95] F. Ajzenberg-Selove, Nucl. Phys. A **433**, 1 (1985); TUNL Nuclear Data Evaluation Project, [http://www.tunl.duke.edu/nucldata/].
[96] D. E. Alburger and A. M. Nathan, Phys. Rev. C **17**, 280 (1978).
[97] A. Strumia and F. Vissani, arXiv:hep-ph/0606054.
[98] J. Engel, E. Kolbe, K. Langanke, and P. Vogel, Phys. Rev. C **54**, 2740 (1996).
[99] E. Kolbe, K. Langanke, and G. Martínez-Pinedo, Phys. Rev. C **60**, 052801(R) (1999).
[100] F. Krmpotić, K. Nakayama, and A. P. Galeão, Nucl. Phys. A **339**, 475 (1983).
[101] H. Budd, A. Bodek, and J. Arrington, arXiv:hep-ex/0308005.
[102] E. Kolbe, K. Langanke, and P. Vogel, Nucl. Phys. A **652**, 91 (1999).
[103] M. Martini, M. Ericson, G. Chanfray, and J. Marteau, Phys. Rev. C **81**, 045502 (2010).
[104] E. Bauer and G. Garbarino, Phys. Rev. C **81**, 064315 (2010).
[105] A. Mariano, E. Bauer, F. Krmpotić, and A. F. R. de Toledo Piza, Phys. Lett. B **268**, 332 (1991).
[106] D. Van Neck, M. Waroquier, V. Van der Sluys, and J. Ryckebusch, Phys. Lett. B **274**, 143 (1992).
[107] A. Mariano, F. Krmpotić, and A. F. R. de Toledo Piza, Phys. Rev. C **49**, 2824 (1994); **53**, 1664 (1996).
[108] R. Lazauskas and C. Volpe, Nucl. Phys. A **792**, 219 (2007).
[109] C. Volpe, J. Phys. G **30**, L1 (2004); arXiv:hep-ph/0303222.
[110] S. E. Woosley, D. H. Hartmann, R. D. Hoffman, and W. C. Haxton, Astrophys. J. **356**, 272 (1990).
[111] M. Th. Keil, G. G. Raffelt, and H.-Th. Janka, Astrophys. J. **590**, 971 (2003).
[112] E. Kh. Akhmedov, presented at Trieste Summer School in Particle Physics, June 7–9, 1999; arXiv:hep-ph/0001264v2.
[113] H. Duan, G. M. Fuller, J. Carlson, and Y-Z. Qian, Phys. Rev. Lett. **99**, 241802 (2007); H. Duan, G. M. Fuller, and Y. Z. Qian, J. Phys. G **36**, 113201 (2009).
[114] K. Nakayama, A. P. Galeão, and F. Krmpotić, Phys. Lett. B **114**, 217 (1982).
[115] M. K. Cheoun, E. Ha, S. Y. Lee, K. S. Kim, W. Y. So, and T. Kajino, Phys. Rev. C **81**, 028501 (2010).
[116] J. S. Bell and C. H. Llewellyn Smith, Nucl. Phys. B **28**, 317 (1971).